BACHELOR

Heat transfer in an once-through boiler for metal fuelled combustion

Siebelt, Tom T.

Award date:
2022

Heat transfer in an once-through boiler for metal fuelled combustion

Bachelor End Project - Report

Department of Mechanical Engineering

T.T. Siebelt - 1253204

Supervisors: H.C. de Lange
H. Ouwerkerk

Eindhoven, January 2022

Abstract

In this thesis research will be done into the usability of iron as a fuel. A boiler needs to be designed in which iron can be burned to iron-oxide where this iron-oxide is not allowed to touch any other metal. this would reduce the effectivity of the boiler because iron-oxide will stick to other metal. Therefore it has been chosen to create a boiler that is a tube in which iron-oxide powder will fall freely down while burning.
This is a continuation on research already done, where the radiation and convection equations where already made. Topics for this thesis are the effect of extinction in the radiation that comes from iron powder in a metal fuelled boiler and the interaction between iron powder and the air inside that boiler. The radiation is modelled using the extinction together with the view factor, this causes the model to not see the other particles. Resulting in a heat transfer only with the wall. So particles will reduce the visibility to the wall but are still ignored when in comes to particle to particle heat transfer. The air to particle heat transfer that is done by convection has also been adjusted. There is a terminal velocity added to the model which results in a boundary layer around the particles and results in larger particles falling through the boiler faster.
The model shows that within the set constraints a boiler can be made that can burn 220 kW of iron. It also shows that one of the important variables is the particle size that is used in the boiler. Large particles will be inefficient in transferring heat and will have a terminal velocity that is too high. But also small particles are in a disadvantage because they will cause a higher extinction of radiation. This behaviour means that there is an optimal size particle.

Contents

List of symbols

Symbol	Variable	Unit
A	Surface area	m^2
A_p	Cross-sectional area of a particle	m^2
A_{pipe}	Cross-sectional area of the boiler tube	m^2
C_D	Friction coefficient	-
c_p	Heat capacity	J/kg·K
D	Particle diameter	m
d_p	Particle diameter	m
Δ	Difference	-
ϵ	Emissivity	-
F	Force	N
$F_{1\rightarrow 2}$	View factor	-
g	Gravitational constant	m/s^2
$\overline{g_i s_j}$	Volume to surface direct exchange area	m^2
γ	Wave length of radiation	m
h_p	Height on the boiler wall	m
h	Convective heat transfer coefficient	W/m^2K
I	Intensity of radiation	W/m^2
k	thermal conductivity	W/·m·K
κ_η	Adsorption coefficient	-
L	Characteristic lenght	m
m_{Fe2O3}	Mass of a iron-oxide particle	kg
$\dot{m}_{air}$	Mass flow of air	kg/s
μ	Viscosity	kg/m·s
μ_t	Extinction coefficient	m^{-1}
$N_{particles}$	Number concentration particles	m^{-3}
Nu_D	Nusselt number for a diameter	-
Pr	Prandtl number	-
ϕ	Angle from the centre of the boiler tube	rad
Q_{ext}	Extinction efficiency	-
Q_{conv}	Convective heat transfer	W
q	Heat transfer	W
σ	Stefan-Boltzmann constant	W/m^2K^4
σ_{sn}	Scattering coefficient	-
Re_D	Reynolds number for a diameter	-
R_r	Average radial length to the wall	m
r_{pipe}	Radius of the boiler tube	m
ρ	Density	kg/m^3
ρ_{Fe2O3}	Density of iron-oxide	kg/m^3
S	Distance to a point on the wall	m
T	Temperature	K
V_i	Volume of a specific particle	m^3
v_{mean}	Mean velocity inside the boiler	m/s
v_∞	Terminal velocity	m/s
w_i	Weight fraction	-
x_p	Point of a particle on the horizontal plane	m

1 Introduction

The idea of using metal fuels came forward out of the search for a new energy-trading commodity by J.M. Bergthorson. In his article (Bergthorson et al., 2015) he describes the current problem, that only carbon based energy carriers are suitable for transportation. For example when considering international trade. However metal based fuels could replace these carbon fuels. It would work by burning for example iron which would create rust. With renewable energy this rust could be transformed into iron again. Storing energy inside iron not only is beneficial for transport, it can also be used as an energy storage for excess renewable energy. When a lot of renewable energy is produced bot the demand is too low this energy can be stored in iron.

At Eindhoven University of Technology the student team Team Solid is designing equipment for this process. Also the university itself is working on this in collaboration with HeatPower. The problem at hand is to make a system in which iron can directly be burned inside a boiler where the heat taken out by converting water into steam. For this system a boiler is needed.

In this thesis the design of a metal fuelled once-through boiler will be discussed. The goal is to come with a design that is able to generate 200 kW of steam. There are several individual problems at play considering the boiler design, which will be discussed later. The mayor uncertainty is the feasibility of a boiler in which radiation is the main driving force in transferring the heat to the steam (Diepstraten, 2021). It is not known how much of the radiation coming form the iron-oxide particles will be adsorbed by other particles before it reaches the wall where it will heat water. In a previously conducted thesis it was assumed that the particles would be a black object (van Leeuwen, 2021). Continuing on that work, now the interaction between particle will be researched.

Furthermore the model made in the previously mentioned theses will be refined by researching previously made assumptions. With this model recommendations will be made about the optimal dimensions for the metal fuelled boiler. In Figure 1.1 the preliminary boiler design can be seen.

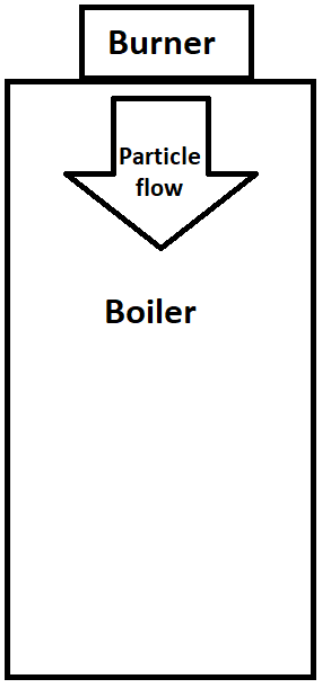

Figure 1.1: Schematic of the boiler tube. **[Original figure redacted]**

2 Problem Statement

This thesis is a continuation of the research done to design a once through boiler in which a iron powder can be burned as fuel. To continue on the research it needs to be known what has been done and it should be clear where the gaps are in that research.
The main objective is finding the optimal variables for the boiler design. This needs to be done by improving upon the existing model. These improvements will be found in the radiation heat transfer and in the convective heat transfer. Also a deeper look will be given to the actual boiler design to see if the current model will be a good approximation.

Radiation adsorption by particles

The radiative heat transfer is modelled as a black object by Van Leeuwen (van Leeuwen, 2021). This however is not entirely true, the particles are blocking each others radiative heat. This behaviour needs to be included in the model. A resulting problem could the feasibility of a boiler in which radiation is the main driving force in transferring the heat to the steam. Resulting in the question: What is the influence of the particles on the radiative heat transfer?

Heat transfer between the particles and the surrounding air

The assumption up to now is that within the boiler all particles will fall with the velocity of the air. The heat transfer does not factor in a boundary layer between the particles and the air because there is no difference in velocity between them. It needs to be investigated if the speed between the air and the particles is negligible or if it needs to added to the model. In the latter case a boundary layer needs to be modelled but also the velocity will influence how fast different size particles will go through the boiler, directly effecting the cooling capability of the boiler. Resulting in the question: How much does the velocity between the air and particles differ and how will this influence the convective heat between them?

Distribution of particles inside the boiler tube

The boiler itself will be build with a burner which does not cover the full diameter of the boiler tube. This will cause the particles to be located only in the middle of the boiler tube. Before it has always been assumed that the particles where everywhere in the boiler tube. But what happens when the particles are not distributed over the whole boiler tube?

2.1 Requirement, preferences and constraints

For the boiler there are several RPC's that need to be taken into account. Most importantly is the constrain that the particles need to be cooled down to 800°C at the end of the boiler.

Table 1: Requirements, preferences and constraints for the metal fuelled boiler.

Requirements	• The power input of iron-oxide should at least be 200 kW. • The boiler should have a diameter of 1 metre up to the steam tubes. • The steam tubes need to produce steam of 180°C.
Preferences	• The power input is preferred to be as high as possible.
Constraints	• The iron-oxide particles need to be cooled down to at least 800°C at the end of the boiler tube. • The boiler can not be higher then 2.5 metres. • The iron powder burner has a radius of 705 milimetres.

3 Used assumptions

Several assumptions are done that are important for the model. However these assumptions do sometimes not reflect reality. In Table 3 the standard variables for the model are stated. These do not always reflect the real world values but will give an approximation.

Boiler properties

The boiler can be seen in Figure 1.1 where some dimensions are given but they do not include some that are at play in the model. The model needs a outer diameter that is not equal to the outer diameter of the actual boiler. The outer diameter of the boiler corresponds with the diameter where the steam tubes are located. These steam tubes are modelled to have the same shape as the boiler wall, while in reality they are tubes inserted on the sides of the boiler. Figure 4.1 shows 1396 mm diameter inside the boiler however only around 1 meter of this will be assumed for the particle flow with its borders being the steam tubes. The boiler is assumed to be 2.5 m long in height which is also different on the sketch.

Model properties

The model is not able to exactly predict the behaviour of temperatures and velocities of the boiler. It assumes that all particles will fall straight down with a certain speed and steam tubes have their temperature set to a constant. Furthermore in Figure 6.1 a heat flow diagram can be seen, these are the only heat flows modelled. So there is no heat transferred to the top and bottom of the boiler. The model assumes they are not seen by the radiation and convection does not interact with it. The model also assumes that because of other particles blocking radiation it can not see the wall/steam tubes. However radiation from particles will not interact with other particles, there is no radiative heat transfer between particles.

There are two models made one continues with the assumption that particles are distributed over the whole boiler. But *model 2* will have the particles only distributed centrally. In *model 2* this will cause a layer of air between the wall and the particles. This layer is assumed to be fully insulating, meaning that there is no convective heat transfer to the wall in *model 2*. Between the air layer and the particles there is no interaction.

Temperature dependent constants

In the model assumptions are made that do not entirely reflect the real situation. This includes the specific heat for air and thermal conductivity of air. These are temperature dependent, so they will change when the temperature changes but in the model they are considered constant. A sensitivity analysis needs to be done to determine the impact of these values.

4 Extinction of Radiation

A mayor influence on the heat transfer in the metal fuelled boiler is the radiation heat transfer. The heat difference between the particles and the wall/steam tubes will result in heat radiation. In the radiation model made available by Van Leeuwen, the medium of particles is assumed to be a black body (van Leeuwen, 2021). This results in a maximum efficiency in radiation heat transfer considering the particle medium. However as stated by Van Leeuwen this assumption is not true. Particles will also interact with each other by exchanging radiation. This will be modelled by determining the *extinction* of the radiation, where the the amount of radiation intensity is calculated that is left over after going through a "cloud of particles".

4.1 Introduction to radiative heat transfer

To give an understanding about the radiative heat transfer in this case, a short explanation is given about the theory used in the existing model. The existing model is based around a numerical solution using the general equation for the radiative heat transfer seen in Equation 4.1 (Welty, Rorrer, & Foster, 2015), where it shows the heat transfer between a iron-oxide particle and the wall/steam tubes denoted by *pipe*:

$$q = \frac{\sigma(T_{iron}^4 - T_{tube}^4)}{\frac{1-\epsilon_i}{\epsilon_i \cdot A_{iron}} + \frac{1}{A_{iron} \cdot F_{1\to 2}} + \frac{1-\epsilon_p}{\epsilon_p \cdot A_{pipe}}} \tag{4.1}$$

With σ [W/m^{2}K^4] being the Stefan-Boltzmann constant, T [K] being the temperature, ϵ [-] being the emissivity of a material, A [m^2] being the the surface area and $F_{1\to 2}$ [-] being the view factor. Together they will calculate the heat transfer (q [W]). In the numerator the heat transfer per square metre is calculated and in the denominator the resistance is calculated by adding the resistance in emission, view factor and absorption respectively.
This is important because the view factor is used to get to a solution for the problem of the particle cloud that is restricting the heat radiation to the to the steam tube.

4.2 Extinction

The radiation coming form the iron-oxide particles is supposed to reach the steam tubes but will also radiate on other particles. To know what amount of radiation will not reach the steam tubes the Beer-Lambert law in Equation 4.2 can be used (Ahmed, 2015). In this equation the intensity of the radiation is determined after it went through a particle cloud with its properties determined by the extinction coefficient.

$$\frac{dI}{dx} = -\mu_t I \quad \xrightarrow[\text{Integrating}]{} \quad I = I_0 e^{-\mu_t x} \tag{4.2}$$

Where μ_t [m^{-1}] is the extinction coefficient; I_0 [w/m^2] is the intensity of the radiation at position $x = 0$; and I [w/m^2] is the intensity at depth x. μ_t is defined by:

$$\mu_t = N \cdot A_p \cdot Q_{ext} \tag{4.3}$$

With N [m^{-3}] the number concentration of the particles and A_p [m^2] the cross-sectional area of a particle. The extinction efficiency Q_{ext} is dependent on the ratio particle size with the wave length. When $d_p/\lambda \gg 1$ it holds that the extinction efficiency is 2 (Modest, 2013). Assuming the heat radiation has a wavelength of 0.8 μm and the smallest particles considered are 10 μm the ratio is larger than 1 but not by a lot. Also other sizes for the wavelength and for the particles exist within the boiler. For now the extinction efficiency will be assumed to be 2.
The extinction coefficient is dependent, as seen in Equation 4.4, on the adsorption (κ_η) an scattering coefficient ($\sigma_{s\eta}$) (Modest, 2013). These coefficients are necessary to understand some of the next steps but are not used in the model.

$$\mu_t = \kappa_\eta + \sigma_{s\eta} \tag{4.4}$$

The number concentration of the iron-oxide (Fe_2O_3) particles inside the combustion chamber can be determined by:

$$N_{particles} = \frac{\dot{m}_{oxide}}{A_{pipe} \cdot v_{mean} \cdot m_{Fe2O3}}, \tag{4.5}$$

with $\dot{m}_{oxide}$ [kg/s] the mass flow of the Fe_2O_3 particles; A_{pipe} [m^2] the cross-section of the boiler pipe; v_{mean} [m/s] the mean velocity of the medium and m_{Fe2O3} [kg] the mass of the iron-oxide particle.

4.2.1 Extinction coefficient in a poly-disperse medium

Due to the use of a poly-disperse medium the extinction coefficient (μ_t) can not be directly determined with Equation 4.3. The distribution of the grades of particle sizes also plays a role and with the weighted average the extinction coefficient can be determined (Ahmed, 2015):

$$\mu_t = \sum_i w_i \mu_t^i \tag{4.6}$$

With w_i [-] the weight fraction of the particle grade in the mixture with its extinction coefficient of μ_t^i. To calculate the extinction coefficient of a particle grade Equation 4.3 can be adjusted to:

$$\mu_t^i = N \cdot A_p^i \cdot Q_{ext} \tag{4.7}$$

Note that N is used and not N_i due to the weighted average being the deciding factor of how much a certain particle grade will influence the total extinction coefficient. To determine the weighted average for every particle the mass of a separate grade needs to be divided by the total mass of all grades:

$$w_i = \frac{N_i \cdot V_i \cdot \rho_{Fe2O3}}{\sum_i N_i \cdot V_i \cdot \rho_{Fe2O3}} \tag{4.8}$$

Where V_i [m^3] is the volume of a particle with a specific size and ρ_{Fe2O3} [kg/m^3] the density of iron-oxide.

4.2.2 Mean distance

From Equation 4.2 it can be seen that the the distance x needs to be known for every point in the boiler. This can be calculated by using the same mathematics used to determine the view factor. Considering the distance in the cross-sectional plane to the boiler tube, a point (x_p) in that plane can be determined by (van Leeuwen, 2021):

$$R_r(x_p, \phi) = x_p \cdot cos(\phi) + \sqrt{r_{pipe}^2 - (x_p \cdot sin(\phi))^2} \tag{4.9}$$

Where ϕ is the angle [rad] between the line to the centre of the boiler tube and to the point on the wall to where the distance needs to be determined. r_{pipe} is the radius [m] of the boiler tube, as can be seen in Figure 4.1. To get the mean distance to the wall of one point in the tube Equation 4.9 needs to be integrated:

$$R_{mean}(x_p) = \frac{1}{2\pi}\int_0^{2\pi} x(x_p, \phi)d\phi = \frac{1}{2\pi}\int_0^{2\pi} x_p \cdot cos(\phi) + \sqrt{r_{pipe}^2 - (x_p \cdot sin(\phi))^2}d\phi \tag{4.10}$$

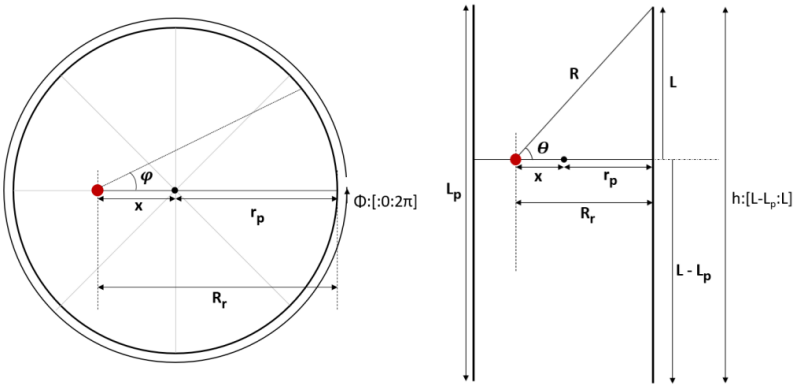

Figure 4.1: Horizontal (l) and vertical (r) cross-sectional sketch of the boiler pipe with the mathematical variables (van Leeuwen, 2021)

This however only works for the cross-section horizontal on the pipe. So this is only valid in the 2D space and not in the real 3D space because also the boiler length needs to be considered. This part again uses the mathematics used by Van Leeuwen in the view factor.
The distance in the length of the boiler can be calculated with the distance from the particle R_r [m] to the boiler wall and from the particle height h [m] to both ends to the tube. Together with the Pythagoras theorem the distance S [m] to a point on the wall can be calculated:

$$S = \sqrt{R_r^2 + h_p^2} \tag{4.11}$$

The Equation 4.10 shows that the mean distance in the horizontal plane can be determined by an integration. This is also true for the height h. It is stated that an integral over the height from $L_{pipe} - L$ to L will suffice to get the mean height (van Leeuwen, 2021). Where L_{pipe} is the total length of the boiler tube and L is the distance from the top to the particle height. Resulting is a total mean beam length determined by:

$$S_{mean} = \int_0^{2\pi} \int_{L-L_{pipe}}^{L} \sqrt{R_r^2 + h_p^2}\, dh d\phi \tag{4.12}$$

4.3 Mean Beam Length Method and Zonal Method

Implementing the extinction is done by using the *Zonal Method*. This is a numerical solution to the *Mean Beam Length Method* which combines the view factor and extinction in one solution to the radiation heat transfer. The view factor and intensity ratio can be multiplied with each other to correct for the particles obstructing the radiative heat transfer. This is stated by the mean beam length method: "The spectral heat flux arriving at and absorbed by dA from a volume element is equal to the spectral emission by dV into all (4π) directions $\times$ the fraction intercepted by dA $\times$ the fraction transmitted along the path from dV to dA" (Modest, 2013):

$$q_\eta dA(\mathbf{r}_w) = \int_V (4\pi\kappa_\eta I_{b\eta} dV) \times \left(\frac{dA\, cos(\theta)}{4\pi S^2}\right) \times e^{-\mu_t S} \tag{4.13}$$

And reduces to:

$$q_\eta(\mathbf{r}_w) = I_{b\eta} \int_V e^{-\mu_t S} \frac{\kappa_\eta\, cos(\theta)\, dV}{S^2} \tag{4.14}$$

Where $q_\eta(\mathbf{r}_w)$ [W] is the heat flux, $I_{b\eta}$ [W] is the emission from the gas considering it is a black body, $\mu_{t\eta}$ [m^{-1}] is the absorption coefficient, S [m] is the distance to the surface. By multiplying the view factor with the intensity factor, which results from the extinction coefficient, a new value for the view factor is created. It describes the view factor of a particle to the wall with the assumption that other particles obstruct his view. What this neglects is that particles do see each other and will also radiate onto other particles, so with this solution they will not exchange energy with each other.

However this would only work for isothermal volumes of hot gasses. Nowadays, with the use of computational power, the numerical *zonal method* can be used, in which the volume and the surface is divided into volume and area zones. For every zone a energy balance is preformed.
When talking about radiative exchange in a gray media there are three ways in which there is a radiative heat transfer; between surfaces, between the volume and surface and between the volumes. Considering all surfaces in the medium are considered the same temperature there won't be any net surface to surface heat exchange. To determine the volume to surface net energy exchange, every volume zone and surface zone $Q_{i\to j}$ [W] needs to be determined (Modest, 2013):

$$Q_{i\to j} = \overline{g_i s_j} E_{bi} \tag{4.15}$$

In which $\overline{g_i s_j}$ [m^2] is the volume to surface direct exchange area with the definition: $\overline{s_i s_j} = A_i F_{i\to j}$. This exchange area can determined by energy emitted from dV_i into all 4π directions $\times$ fraction leaving toward dA_j $\times$ fraction transmitted (Modest, 2013). Which leads to:

$$(4\kappa_\eta E_{bi} dV_i) \times \left(\frac{dA_j\, cos(\theta_j)}{4\pi S^2}\right) \times e^{-\mu_t S} \tag{4.16}$$

And reduces to:

$$\overline{g_i s_j} = \int_{V_i} \int_{A_j} e^{-\mu_t S} \frac{cos(\theta_j)}{\pi S^2} \kappa_\eta dA_j dV_i \tag{4.17}$$

This shows that the extinction can be integrated in the integral that determines the view factor $F_{i\to j}$. However in the model that will be made, only volume to surface is considered and not also volume to volume to make the model simpler. Also the energy emitted is determined differently so the μ_t will not be in the integral a second time, so it will only be in the exponent of e. So taking out the energy emission leads to:

$$\left(\frac{dA_j \ cos(\theta_j)}{4\pi S^2} \right) \times e^{-\mu_t S} \tag{4.18}$$

And reduces to:

$$\overline{g_i s_j}^* = \int_{A_j} e^{-\mu_t S} \ \frac{cos(\theta_j)}{4\pi S^2} dA_j \tag{4.19}$$

Where $\overline{g_i s_j}^*$ [m^2]resembles the volume to surface direct exchange area without the emission factor. The term $\frac{cos(\theta_j)}{4\pi S^2}$ resembles the view factor before the integration over the area. This part can be replaced with the view factor applicable to the current problem (van Leeuwen, 2021):

$$F_{12}(R_r, \phi, h_p) = \frac{1}{\pi} \int_0^{2\pi} \int_{L-L_p}^{L} \frac{R_r^2 \cdot r_{pipe}}{\pi \cdot (R_r^2 + h_p^2)} dh d\phi \tag{4.20}$$

Where $R_r(x_p, \phi)$ is described in Equation 4.9. As can be seen the cylindrical coordinate system needs to be used which replaces the $\int_{A_j} dA_j$. Resulting in the final equation with which the fraction of energy that will reach the wall will be solved:

$$\overline{g_i s_j}^* = \frac{1}{\pi} \int_0^{2\pi} \int_{L-L_p}^{L} e^{\mu_t \sqrt{(R_r^2+h_p^2)}} \frac{R_r^2 \cdot r_{pipe}}{\pi \cdot (R_r^2 + h_p^2)} dh d\phi. \tag{4.21}$$

Where previously S was used for the length an energy ray had to travel trough the medium, it now is defined by $S = \sqrt{R_r^2 + h_p^2}$, the average length a ray has to travel described in Equation 4.11.

5 Heat Transfer due to Convection

There are two places where convection plays a role in the boiler. The iron-oxide particles and the air have a convective relation and the air also transfers heat due to convection with the wall/steam tubes. In the previous model the convection between the particles and the air was assumed to be optimal, meaning that there was no boundary layer between them and that the air and the iron oxide particles fell through the boiler at the same velocity. This velocity will be decoupled in this section so the convection can be determined more precisely. To determine the convection between the air and the particles the Nusselt number needs to be known. Therefore the terminal velocity needs to be determined, this is the velocity of a particle compared with the air. Meaning that the total velocity of that particle is the terminal velocity plus the air velocity. With the terminal velocity a Reynolds number can be determined which is used to get a Nusselt number.
This section will also include the numeric solution for the convective heat transfer between the iron-oxide particles and the air. This solution had to be found using the *Euler Implicit Method* due to an otherwise unstable model.

5.1 Introduction to convection

The convective heat transfer is defined by Equation 5.1 where the Q is the convective heat transfer [W], h is the convective heat transfer coefficient [W/m^{2}K], A is the area [m^2] over which heat is transferred and ΔT is the difference in temperature [K] of a fluid and a solid body transferring heat.

$$Q_{conv} = h \cdot A \cdot \Delta T \tag{5.1}$$

When the fluid has a velocity compared with the body a boundary layer will form between the bodies. This boundary layer will have an influence on the convective heat transfer, when a boundary layer forms it will work as a insulating layer resulting in a reduction of the convective heat transfer coefficient. In the next sections it is described how this heat transfer coefficient is determined when working with a boundary layer.

5.2 Terminal velocity

The first step in determining the convective heat transfer is to determine the terminal velocity. This is the maximum velocity of an object when it falls through a fluid. To determine this maximum, the friction force and the gravitational force need to be used. The gravitational force is the force resulting in the particle to fall but at a certain speed the friction force will become just as high as the gravitational force and therefore they will be in equilibrium. This speed at which those forces are in equilibrium is called the terminal velocity. The terminal velocity v_∞ is determined by (Welty et al., 2015):

$$\frac{F}{A_p} \equiv C_D \frac{\rho v_\infty^2}{2}, \tag{5.2}$$

where F is the force [N] due to friction, A_p is the projected area [m^2] of the object, C_D is the friction coefficient [-], ρ is the fluid density [kg/m^3] and v_∞ is in this case the terminal velocity [m/s]. The force due to friction will need to equal the force on the object due to gravity to come to a equilibrium and so a constant terminal velocity:

$$F = \rho_s \frac{\pi d^3}{6} g = C_D \frac{\rho_f v_\infty^2}{2} \frac{\pi d^2}{4}, \tag{5.3}$$

leading to:

$$C_D v_\infty^2 = \frac{4\rho_s}{3\rho_f} dg. \tag{5.4}$$

5.2.1 Drag coefficient

For the next part the drag coefficient C_D needs to be determined. This coefficient is a function of the Reynolds number ($C_D = f(Re)$). The function differs for every shape and is often approximated for

example for spheres it holds that when the Reynolds number is small ($Re \ll 1$) the Stokes drag can be used: $C_D = \frac{24}{Re}$. This is due to a linear relation between the drag coefficient and the Reynolds number when $Re \ll 1$. The Reynolds number can be seen in Equation 5.9, resulting in the equation:

$$v_\infty^2 = \frac{4\rho_s}{72\mu} d^2 g \tag{5.5}$$

But this changes when the Reynolds number becomes larger. It was found that the iron-oxide particles used would have a variety of Reynolds numbers that would not always be a lot smaller than one and also to be able to run the model using larger particles a better estimation for C_D needs to be found. The estimation:

$$C_D = \frac{23.5}{Re_D} + \frac{4.6}{\sqrt{Re_D}} + 0.3, \tag{5.6}$$

is used to for Reynolds numbers between 10^{-2} and 10^5 (Yow, Pitt, & Salman, 2005). This can be used in Equation 5.4 to make a solvable solution for the terminal velocity. For this the Reynolds numbers need to be filled in according to Equation 5.9 where $v = v_\infty$, solving for v_∞ results in the terminal velocity.

5.2.2 Nusselt number

With the terminal velocity determined it is now used to get a value for the boundary layer between the particle and the air. This value is the Nusselt number defined by $Nu = \frac{hL}{k}$, so its the ratio of the convective (h) and conductive (k) heat transfer coefficients. The L is the characteristic length which determines boundary layer. The Nusselt number can also be determined with other functions for example in Equation 5.7 (Whitaker, 1972), which are approximations based on observations. The advantage of this is that for every boundary layer the heat transfer coefficient (hL) can be determined by multiplying the Nusselt number with the conductive heat transfer coefficient: $hL = Nu \cdot k$. This way a boundary layer can be included in the heat transfer.

$$Nu_D = \frac{hL}{k} = 2 + (0.4Re^{1/2} + 0.06Re^{2/3})Pr^{0.4} \left(\frac{\mu_\infty}{\mu_w}\right) \tag{5.7}$$

Where μ_∞ is the viscosity evaluated at the mean bulk temperature and μ_w is the viscosity evaluated at the mean wall temperature. But also the approximation:

$$Nu_D = 2 + 0.6Pr^{1/3}Re_D^{1/2}, \tag{5.8}$$

has been found (Young & Pfender, 1987), which is simpler to use. These equations are dependent on the Reynolds and Prandtl numbers:

$$Re_D = \frac{Dv\rho}{\mu}, \tag{5.9}$$

$$Pr = \frac{\mu c_p}{k}, \tag{5.10}$$

respectively. Where D is the diameter [m] of the particle, v is the velocity [m/s] relative between the particle and the fluid, ρ is the density [kg/m^3] of the fluid, μ is the viscosity [kg/m·s] of the fluid, c_p is the heat capacity [J/kg·K] of the fluid, k is the thermal conductivity [J/s·m·K] of the fluid and h is the heat transfer coefficient [J/s·m^2·K].

5.2.3 Implications of the terminal velocity

The terminal velocity, v_∞, adds extra velocity to iron-oxide particles going through the boiler tube. Not only will this have an implication for the convective heat transfer, it also effects other calculations like the one for the particle concentration , $N_{particles}$, in Equation 4.5. In Equation 5.11 the new equation is written:

$$N_{particles} = \frac{\dot{m}_{oxide}}{A_{pipe} \cdot (v_{mean} + v_\infty) \cdot m_{Fe2O3}} \tag{5.11}$$

This will reduce the particle concentration and then also resulting extinction. But the terminal velocity also causes large particles to fall through the boiler faster, leading to larger particles having spend less time in the boiler and therefore have less time to cool down.

5.3 Implementation

Going back to the principles of convective heat transfer in Equation 5.1 it can be seen that an equation can be made with the information gathered above:

$$\begin{aligned} Q_{conv} &= h \cdot A \cdot \Delta T \\ &= Nu \cdot k_{air} \cdot 2\pi \cdot r_{Fe2O3} \cdot (T_{particle} - T_{air}) \end{aligned} \tag{5.12}$$

With this heat transfer in wattage the temperature of a particle can be determined. For this the convective heat transfer value needs to be expressed in Kelvin. With that the reduction in temperature can be determined.

$$\Delta T_{conv} = \frac{Nu \cdot k_{air} \cdot 2\pi \cdot r_{Fe2O3} \cdot (T_{particle} - T_{air})}{c_{p,Fe2O3} \cdot m_{Fe2O3}} \cdot \frac{dh}{(v_{Air} + v_{\infty})} \tag{5.13}$$

Where $c_{p,Fe2O3} \cdot m_{Fe2O3}$ calculates the amount of joules that are needed to change the temperature by one Kelvin. The part: $\frac{dh}{(v_{Air}+v_{\infty})}$ will give the time in seconds that the heat transfer will take place, where dh is the distance along the height where the heat transfer is calculated.
This equation can be extended to also include the temperature delta due to the radiative heat transfer. By adding the radiative heat transfer Q [W] to the convective heat transfer, both will be used to get the total reduction in temperature:

$$\Delta T_{tot} = \frac{(Q + Nu \cdot k_{air} \cdot 2\pi \cdot r_{Fe2O3} \cdot (T_{particle} - T_{air})) \cdot dh}{c_{p,Fe2O3} \cdot m_{Fe2O3} \cdot (v_{Air} + v_{\infty})} \tag{5.14}$$

5.3.1 Implicit Euler method

To calculate the heat transfer between the particles and the surrounding air a numerical solution needs to be found. This solution is given by the Implicit Euler Method (Butcher, 2016) seen in Equation 5.15 with step size dh.

$$y_i = y_{i-1} + dh \cdot f(y_i) \tag{5.15}$$

Note that it is written in most literature as a $y_{n+1} = y_n + dh \cdot f(y_{n+1})$, but due to the use case in this model, where the point that is calculated is defined as i, it was adjusted. The reason the implicit Euler method needs to be used here is because the explicit variant will be unstable or the step size needs to be really small resulting in a long simulation time. To calculate the heat transfer convection with a boundary layer Equation 5.16 will be used.

$$T_{p(i,j)} = T_{p(i,j-1)} - \frac{(Q_{(i,j)} - Nu \cdot k_{Air} \cdot 2\pi \cdot r_{Fe2O3} \cdot (T_{Air(i.j-1)} - T_{p(i,j)})) \cdot dh}{c_{p,Fe2O3} \cdot m_{Fe2O3} \cdot (v_{Air(i,j-1)} + v_{\infty})} \tag{5.16}$$

Where i and j are the numerical calculation points along the width and height of the boiler respectively, T_p is the temperature of the particle [K], $\dot{Q}$ is the radiation heat flow [W], Nu is the Nusselt number [-], k_{Air} is the thermal conductivity of air [W/m K] , r_{Fe2O3} is the radius of iron-oxide particle [m], $T_{Air(i.j-1)}$ is the temperature of the air [K], $c_{p,Fe2O3}$ is the specific heat of iron-oxide [J/kg K], m_{Fe2O3} is the mass of the iron-oxide particle [kg], $v_{Air(i,j-1)}$ is the velocity of the air through the pipe [m/s] and v_{∞}) is the terminal velocity of the particles compared with the air [m/s]. To find $T_{p(i,j)}$ or in Equation 5.15 y_i this formula needs to be rewritten resulting in:

$$T_{p(i,j)} = \frac{T_{p(i,j-1)} - \frac{(Q_{(i,j)} - Nu \cdot k_{Air} \cdot 2\pi \cdot r_{Fe2O3} \cdot T_{Air(i.j-1)}) \cdot dh}{c_{p,Fe2O3} \cdot m_{Fe2O3} \cdot (v_{Air(i,j-1)} + v_{\infty})}}{1 + \frac{Nu \cdot k_{Air} \cdot 2\pi \cdot r_{Fe2O3} \cdot T_{Air(i.j-1)} \cdot dh}{c_{p,Fe2O3} \cdot m_{Fe2O3} \cdot (v_{Air(i,j-1)} + v_{\infty})}} \tag{5.17}$$

6 Model

The model of the boiler has a few specific uses and assumptions. The main use of the model to calculate the temperature of the iron-oxide particles, so an end temperature can be determined. Also will this model tell something about the sensitivity of certain variables and how certain variables influence the model. First a model needs to be made using the equations from previous chapters and from the theses made by Van Leeuwen and Diepstraten.
In total two models were made, one that works with all particles evenly spread out over the total boiler tube. And one in which the particles are centrally located in the tube. These models are added in Appendix A.

6.1 Distribution of particles over the boiler tube

As stated above two models have been made. This was done because of the assumption that the iron-oxide particles will be homogeneously distributed over the boiler pipe. However as can be seen in Figure 1.1, the burner on top of the boiler does not have the same diameter as the tube, therefore will the assumption for the particle distribution be flawed. This model is called *model 1* from now on.

To give a more realistic view of the problem a second model (*model 2*) was made. Where *model 1* has a particle distribution over the whole boiler pipe, has *model 2* the distribution in the middle of the tube. It can be seen as a centrally located "tube" in which the particles are evenly distributed. This "tube" has no walls and effectively does nothing more than holding the particles centred. *Model 2* was made by making the outer diameter of the boiler tube the diameter of the particle "tube". Meaning that everything is modelled like a really small boiler tube, but by keeping the view factor as before because the outer wall will not change so it is still there to collect radiative heat. Also the convective heat transfer with the wall needs to be taken out of the equation. Because it is assumed that the air layer between the particles and the boiler wall is large enough to insulate the particles from the wall. This makes the script easier because now this air layer does not need to be modelled.

The view factor in Figure B.1a is reduced drastically using this model. This is not due to the extinction of the radiation, which is included in the view factor. At first sight this would seem logical because the same amount of particles need to go through a smaller diameter. But the air speed and the diameter are connected with each other. Due to the oxidation of the iron particles a certain amount of air is needed to provide for the oxygen. So the same amount of air needs to go through a smaller diameter, resulting in a higher velocity as can be seen in Equation 6.1. Together with Equation 5.11 it can be seen that when the terminal velocity is assumed to be negligible ($v_\infty \approx 0$) the cross sectional area of the particle tube (A_{pipe}) is cancelled out.

$$v_{mean} = \frac{\dot{m}_{air}}{\rho_{air} \cdot A_{pipe}} \tag{6.1}$$

Resulting in a particle density which is independent of the area, so diameter, where the particles flow through. This is not entirely true because the terminal velocity is not dependent on this area, but this velocity is not so large it has a lot of impact. The reduced view factor in Figure B.1b is there because the view factor far away from the boiler wall was always the lowest. Also in *model 1* it is quite low when the view factor is taken near the middle of the boiler tube.

6.2 Important working mechanisms

In the models there are several mechanisms that cause interesting behaviour. Understanding this behaviour is then crucial to design a metal fuelled boiler.When talking about working mechanisms in the boiler design, first the already mentioned radiation and convection will come up. To describe what has been done Figure 6.1 shows the heat flows caused by these main working mechanisms. Noticeable is that convection between the particles and the air is actually the air heating up the particles. This is because the air is a laminar flowing fluid and heat conduction through the air to the wall is small compared with the radiation going to the wall. Therefore radiation is cooling down the iron-oxide particles, resulting in the hot air heating them up again.

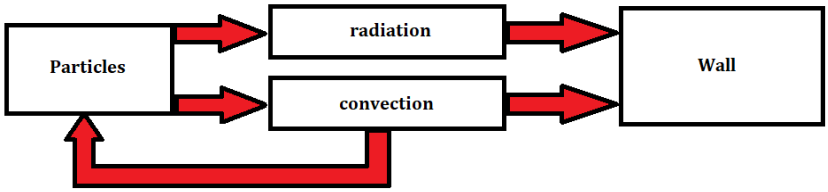

Figure 6.1: Radiation and convection as with its heat flows as modelled in *model 1*.

Implications of this is that small particles will be hotter because their contact area versus mass is higher than large particles. But this also means that small particles will transfer more heat by radiation to the wall. Small particles cool down the medium faster. But within this mechanism there are two more mechanisms at play. These are the extinction and terminal velocity.
In Figure 6.1 the heat flows for *model 1* are shown. To get the heat flow for *model 2* the arrow between the convection and the wall needs to be removed because of the outer air layer working as an insulator.

6.2.1 Terminal velocity

The terminal velocity is given by Equation 5.4 where it can be seen that larger particles will fall faster. For a simplified view the Stokes drag can be used as in Equation 5.5. It shows a linear relation. When the drag coefficient (Equation 5.6) is looked at, it shows that it does not give a linear relation but:

$$v_\infty \propto \sqrt{d^2 + d^{\frac{3}{2}}} \tag{6.2}$$

Which could be assumed linear for low diameters. When the large particles are used the terminal velocity goes up. However the implication of it is that large particles will not only be less effective in cooling down the medium as discussed before, but also will spent less time in the boiler and therefore they will contribute less to the total heat transfer.

6.2.2 Extinction

The extinction of the radiation causes some interesting behaviour. Where before the negative implications considering the particle size would only hold for relative large particles, now this will also have a negative implication for very small particles.
In Equation 4.3 and Equation 5.11 the equations for the extinction coefficient and the particle concentration are shown. When taken those together with the formula for the mass of a particle ($m_{Fe2O3} = 4/3\pi \cdot \rho_{Fe2O3} \cdot r_{Fe2O3}^3$) and the cross sectional area of a particle ($A_p = \pi \cdot r_{Fe2O3}^2$) the effect of the particle size can be determined. When talking about small particles the terminal velocity can be neglected ($v_\infty \approx 0$), which makes the equation easier to understand:

$$\mu_t = \frac{\dot{m}_{oxide} \cdot \pi \cdot Q_{ext}}{A_{pipe} \cdot v_{mean} \cdot 4/3\pi \cdot \rho_{Fe2O3}} \cdot \frac{1}{r_{Fe2O3}} \tag{6.3}$$

It is important to remember that a low extinction coefficient is preferred, meaning that small particles will increase the extinction coefficient. Meaning that when only very small particles are used, the radiation heat transfer will be reduced. Considering the extinction coefficient is an exponent of e (Equation 4.21) this will be a exponential relation. So it has the potential to have a lot of influence on the heat transfer.

6.2.3 Implications for the model

The heat transfer and terminal velocity will cause large particles to be less effective on one side but the extinction will cause small particles to be less effective. Therefore there needs to be an optimum particle size. A particle distribution around this particle size will result in the best performance. Considering the extinction works as an exponent the distribution should most likely have a sharper slope on the side of the small particles.

6.3 Sensitivity analysis

Both models are approximately the same. *Model 1* will be calculate the heat transfer when the whole tube is filled with iron-oxide particles, so the particles are fully along the tube. *Model 2* will however have the particles only distributed in the centre of the tube. For the air properties the model uses constants however some are temperature dependent. The Specific heat (C_p), viscosity (μ) and thermal conductivity (k) are constants in the model. In Table 2 the outer values for these values are written down. Furthermore also the particles size distributions need to be analysed

Table 2: Temperature dependent properties of air, taken as a constant in the Model.

Temperature [°C]	C_p [J/kg K]	μ [Pa s]	k [W/m K]
800	1154	4.332e-5	7.135e-2
1200	1207	5.205e-5	9.053e-2

6.3.1 Temperature dependent constants

The test was done one time with all the variables from 800°C and one time with all the variables from 1200°C. They were not tested separately because the importance of this analysis is to know the influence on the model and its dependence on the temperature in a whole. Not all properties individually. It can be seen in Figure A.1 and Figure A.2 that the extremes of the variables for air have some influence on the temperature curve, but do not make a lot of difference. The values for the low temperature gave an end temperature that was a bit higher.
When changing the specific heat of iron-oxide the temperature curve did not change a lot. For the specific heat there was no value found depending on other temperatures. To still know if a different specific heat would influence the model it was adjusted it in both directions by 20%. This did not resulted in high differences.

Also in the centrally distributed model (*model 2*) a similar behaviour is shown when the air properties are adjusted. In Figure A.3 and Figure A.4 a small difference in temperature is shown.

6.3.2 Particle size distribution

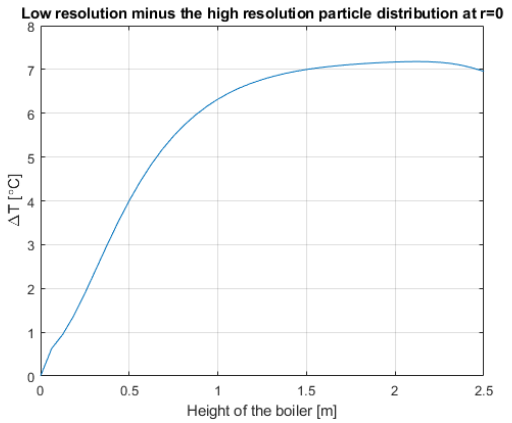

Figure 6.2: Temperature difference (ΔT) where the low resolution is compared to the high resolution along the height of the boiler. The measurement is done in the centre of the boiler so where the radius is zero. (*model 1*)

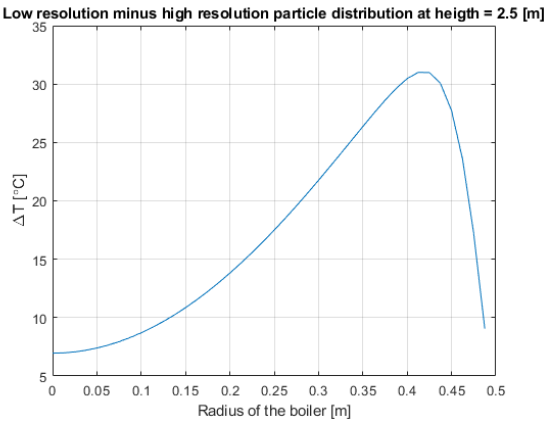

Figure 6.3: Temperature difference (ΔT) where the low resolution is compared to the high resolution along the radius of the boiler. The measurement is done at the end/bottom of the boiler so where the height is defined as 2.5 [m]. (*model 1*)

For the model two different types of particle distributions are used. To model a few easy to differentiate particle sizes there is a low resolution particle distribution in Table B.1, made up out of 6 particle sizes. There also is one made out of 25 sizes, this one is a measurement done at the TU/e on a sample

of a iron powder that can be bought on the market. To see if this higher resolution distribution is similar to the low resolution one they need to be compared. For *model 1* the comparison resulted in a maximum temperature delta that was around 7°C when comparing the centre of the boiler tube as can be seen in Figure 6.2. However the along the radius of the boiler the temperature deltas are over 30°C as can be seen in Figure 6.3. *Model 2* has also been checked in the same way and had similar results however the maximum temperature deltas were a bit lower as can be seen in Figure A.5 and Figure A.6.

These values have been recorded using the standard variables described in Table 3. Changing those variables could also influence the accuracy of the model concerning the particle distribution. Therefore it is wise to use the high resolution always to get actual values from the model.

7 Results

For the next part all variables in the model are discussed and researched to find their influence on the model. Using this data a optimal boiler design within the given requirements and constraints can be found. First a selection of the main results are shown in section 7.1. The variables could be divided into three subcategory: particle distribution, thermodynamic and physical variables. Where the first one, particle distribution, will be split in two sections where in one a mono-disperse grade is used to find the optimal particle size.

7.1 Main Results

The main results of the model are taken with all the standard values applied to the model. These are listed in Table 3. The used particle distribution can be found in Table B.1. This distribution is low resolution but is useful when comparing different particle sizes. However there is also a higher resolution distribution that gives a more accurate representation of the temperature curve found in Table B.2. Temperature curves from both resolutions are however very similar and deviate a maximum of 7°C as can be seen in section 6.3. So for comparison graphs the low resolution distribution will be used, but numbers will be taken out of the high resolution particle distribution. However this 7°C difference is only true for results that are taken at the centre of the boiler tube. This is also where the temperature is the highest and therefore also the focus of all temperature values. All final temperatures are taken in the centre of the boiler.

Table 3: Standard values for the variables in the model. (*Only applicable for *model 2*)

Power input	Heating value	Starting temperature	Steam pipe temperature
200 kW	$5.2 \cdot 10^6$ J/kg	1200 °C	180 °C
Boiler tube radius	Boiler tube length	Specific heat air	Density air
0.5 m	2.5 m	1134 J/kg·K	0.369217 kg/m^2
Viscosity air	Thermal conductivity air	Specific heat Fe_2O_3	Density iron
$4.0549275 \cdot 10^{-5}$ Pa·s	$6.573 \cdot 10^{-2}$ J/kg·K	654 J/kg·K	7860 kg/m^2
Density Fe_2O_3	Emissivity iron	Particle tube radius*	
5242 kg/m^2	0.85	0.3 m	

In Figure 7.1 the temperature curve of *model 1* can be seen. This is the temperature at the core of the boiler and progresses on the x-axis down alongside the height of the boiler. Where the top of the boiler is at $x = 0$, and down is the positive direction. The resulting air temperature at $x = 2.5$ will be 719°C. In Figure 7.2 the temperature curve for *model 2* is given, measured the same way as in *model 1*. The resulting air temperature here will be 892°C.

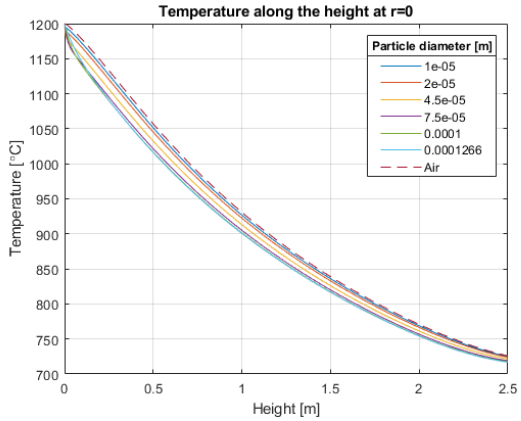

Figure 7.1: Temperature curve of *model 1* using the standard values from Table 3.

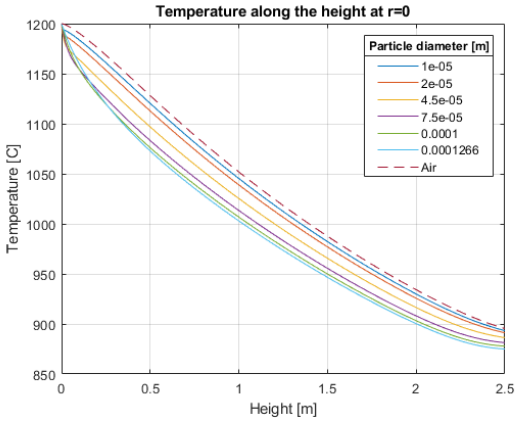

Figure 7.2: Temperature curve of *model 2* using the standard values from Table 3

These results assume are given by two different models. In *model 1* the view factor is higher as can be seen in Figure B.1 and there is convection with the wall possible. In *model 2* this is not the case and therefore the end temperature is higher. These temperatures are two extremes because *model 2* is a quite pessimistic model and therefore the actual end temperature could very well be in between the 719°C and 892°C. Definitely considering that the particle tube radius is taken to be 0.3 metres. However the iron powder burner can give a swirl to the particles making the medium rotate around the vertical axis. With that swirl a centripetal force will cause the particles to move to the wall, resulting in a bigger particle tube while going down the boiler. However modelling this would be outside the scope of this thesis.

More things can be done to improve the temperature curve, which is for *model 2* especially needed considering that the end temperature is outside the constrains. So the optimal working conditions for these models need to be found.

7.2 Mono-disperse behaviour

To research the behaviour of the particle size and to find the optimal particle the poly-disperse grade of Table B.1 is changed to be six mono-disperse grades with the same sizes used for the poly-disperse grade. With these six grades the behaviour of a single type of particle can be modelled and analysed.

For *model 1* the mono-disperse grades can be seen in Figure 7.3 but is shows some counter intuitive behaviour compared with the poly-disperse grade, where the highest radius particle will have the lowest temperature. The mono-disperse grades however show that those particles have the highest temperature. This behaviour can be put in context when looking at the effectivity of the particles at reducing the temperature of the medium. This was explained in section 6.2 where it states that because of its surface to volume ratio the smaller particles will heat up faster compared to the larger particles and therefore emit more radiative heat. So when using a mono-disperse grade this translates in large particles dissipating less heat and so they will stay in a hotter medium. Therefore also being hotter themselves.
It also shows a that the particle with a diameter of $2 \cdot 10^{-5}$ m has the lowest temperature but that is not the smallest particle. The temperature decreases when smaller particles are used, but at a certain point this does not hold anymore. The smallest particle used has a higher temperature suggesting that there is a optimum around $2 \cdot 10^{-5}$ m. This optimum was explained in section 6.2.3 and in short it holds that a medium of small particles is effected more by the extinction then large particle, creating less radiative heat transfer for small particulate media.

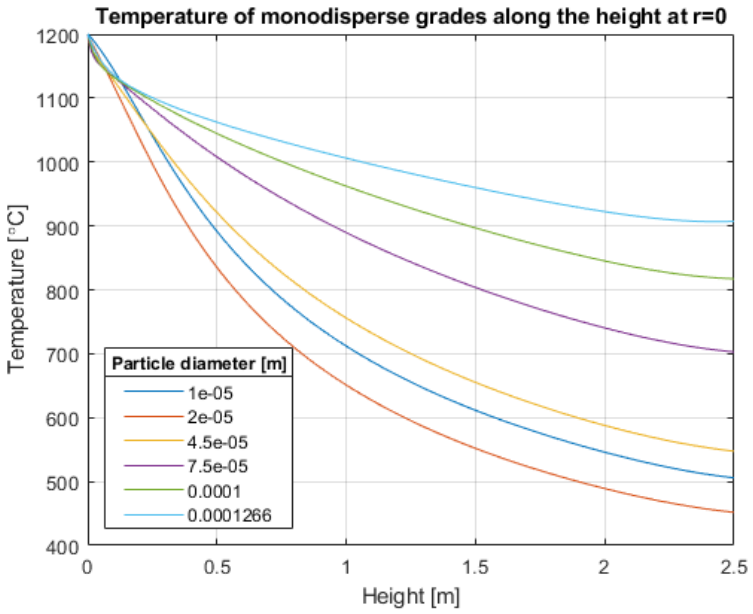

Figure 7.3: Temperature of mono-disperse grades in *model 1*.

The same test as in Figure 7.3 has been done with *model 2*. It shows in Figure 7.4 that the optimal size has become smaller, now the smallest grade has the best result which is particle with a diameter of $1 \cdot 10^{-5}$ m. Considering that the two smallest particle grades are so close together compared with the other grades, it suggests that the optimal particle size will be around that point.

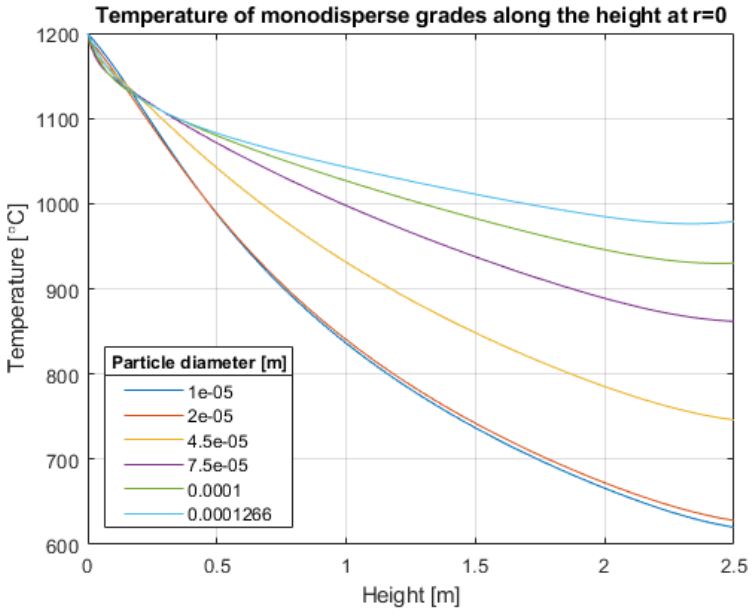

Figure 7.4: Temperature curves of mono disperse grades in *model 2*.

7.2.1 Effect of extinction and terminal velocity

In section 6 it was determined that the extinction and terminal velocity have a theoretical impact on the cooling capacity of the particles. To see of this actually is happening in the model and to see how much if true, the mono-disperse grades are taken and compared with that same grade without the terminal velocity or extinction.

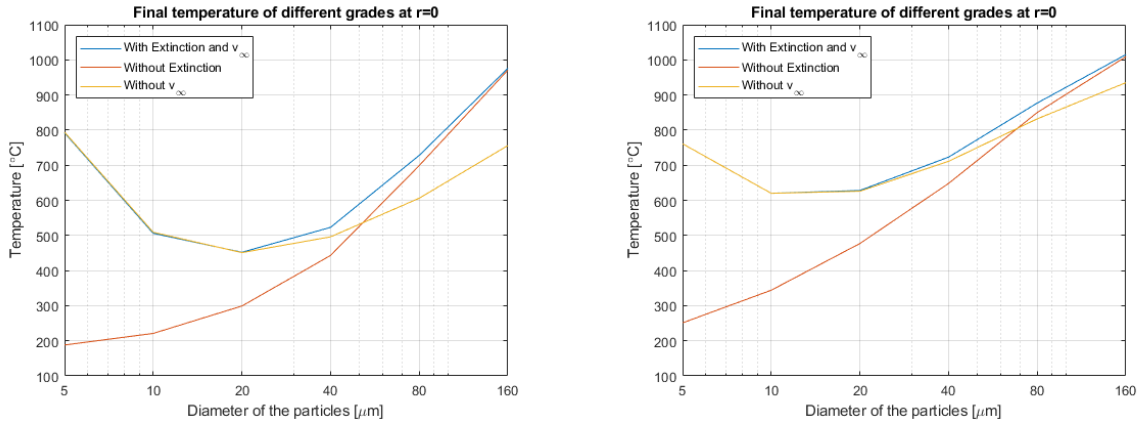

(a) *Model 1* (b) *Model 2*

Figure 7.5: The final temperature of the particles at the end of the boiler for mono-disperse grades. Using particles with a diameter of 5, 10, 20, 40, 80 and 160 μm, with the extinction or terminal velocity (v_∞) taken out of the equation.

To validate that the trend in Figure 7.3 continues with lower diameter particles a none existing mono-disperse grade with a diameter of 5 micrometer is used. It shows an end temperature of 792°C, confirming that this is a continuing trend. Noticeable differences between a diameter of 5 and 100 micrometer

is the extinction coefficient which is around 8 and 0.2 respectfully and the terminal velocity that is higher for the larger particles. Showing that also the model agrees with the theory in this regard. In Figure 7.5 it can be seen that when the particles become smaller there is a large effect by the extinction causing the temperature to rise again. While when the extinction is ignored the temperature curve keeps going down. The effect of the terminal velocity is also shown and it shows that a higher radius means a higher influence of the terminal velocity on the temperature curve. However this is not all the reason for the temperature to go up, because there is still a jump in temperature that does not relate to the terminal velocity. This can be explained by the higher efficiency of small particles in dissipating heat discussed before.
In Figure 7.5b the optimal temperature for *model 2* can be seen. But because there are two values close to the optimal diameter, the diameter of $15 \cdot 10^{-6}$ m has been tested as well. It resulted in a temperature of 612°C also close to the other two values, but a bit lower. This is from now considered to be the optimal diameter for *model 2*. For *model 1* this would be $20 \cdot 10^{-6}$ m. It is also noticeable that for both models the temperature corresponding to the small and large particles is quite similar. Only around the optimum there is a large difference.

In Figure B.2 and Figure B.3 the temperature curves considering the extinction and terminal velocity can be seen for several particle diameters.

7.3 Particle distribution

In the previous sections it has been determent that the particle distribution would have an optimal size considering the temperature curve. Around 1.5 μm it would have the best results considering *model 2*. To evaluate this the distribution has been moved to the left so a higher concentration of particles can be found around the optimal size. The distribution has also been made smaller so all values are more around the optimal point. It can be compared with the original distribution in Figure 7.1 and Figure 7.2 for the *model 1* and *model 2* respectively.
Adjusting the particle distribution was done by changing the particle sizes and not the particle fractions. They are still the same as in Table B.1.

7.3.1 Distribution in *model 1*

Starting the research for the optimal distribution for *model 1* it is first useful to know how the model reacts on changes. It can be seen in Figure B.4a that when the distribution is moved to the right by -5 μm it has a comparable temperature curve as Figure 7.1. This could be explained by the particles with the low diameter of 5 μm which has a large impact on the extinction. However this is not the case because when that value is not adjusted in Figure B.4b it gives a similar temperature curve. The explanation for this is most likely that the number fraction of the smallest particle is very low, so there are not a lot of those small particles. Therefore it is most likely not having a mayor influence on the model no matter its value.
When the diameter is adjusted with an increasing value like in Figure B.4c, it shows a higher temperature drop, showing that the high diameter values have a significant influence. But in Figure 7.6 it also shows that when the same increasing values are used but starting with the second smallest grade, the temperature curve is similar to Figure B.4c. This way the particles in the distribution are larger but still give the same result.

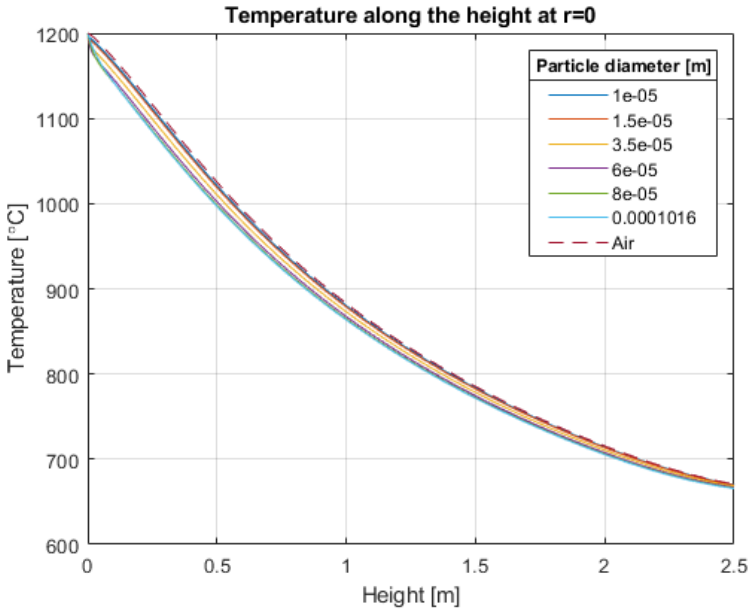

Figure 7.6: Temperature where the particle diameter has been adjusted with an increasing value starting at the second smallest particle (*model 1*).

7.3.2 Distribution in *model 2*

When preforming the same tests on *model 2* it became apparent that the same behaviour can be seen from *model 2* as *model 1* as can be seen in Figure B.5. Using a poly-disperse grade that is narrower around a lower size is beneficial to the temperature curve. Especially filtering out the bigger size particles will improve the boilers performance. The mono-disperse grade test in Figure 7.5b shows that particles with a diameter around 15 μm will have the optimal size so extinction of the radiative heat and the terminal velocity is minimal and the convective heat transfer between the particles and air is still high.
In Figure 7.7 an imaginary grade has been made that will keep the temperature under 800°C and the power input is still 200 kW. This was done by reducing the size of all grades except for the one with the smallest size. A different approach was taken in Figure 7.8 where also a grade was created that would suffice the constraints of end temperature and power input, but now only reducing the size of the largest three grades. This to show that mostly the larger particles cause the higher temperatures and that if those could be reduced this design would work too.

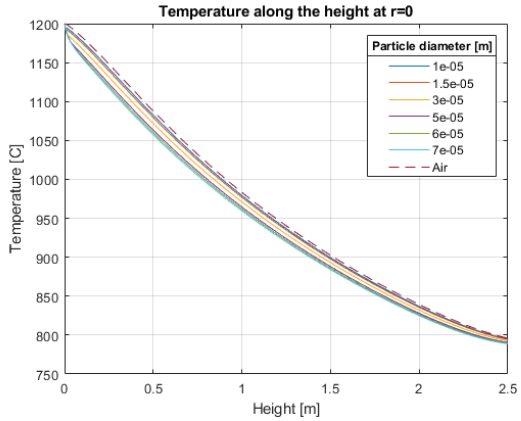

Figure 7.7: Temperature curve of an imaginary grade that would suffice the constraints set by shrinking the 5 highest grades (*model 2*).

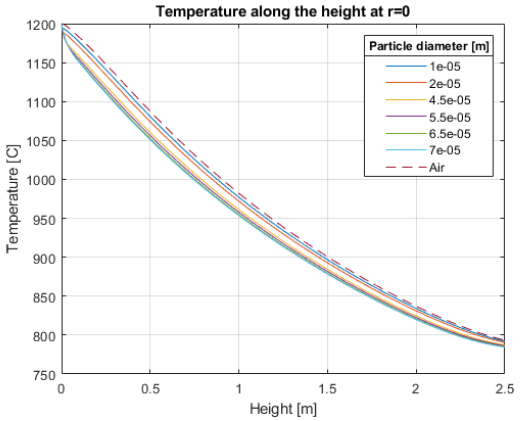

Figure 7.8: Temperature curve of an imaginary grade that would suffice the constraints set by shrinking only the 3 highest grades (*model 2*).

7.4 Behaviour of thermodynamic variables

The thermodynamic variables are the input power, the start temperature of the particles and the temperature of the wall/steam tubes. These variables influence the model in several different ways. So is the input power also responsible for the amount of particles in the boiler. When more power is inputted that also means that more iron needs to be burned. The start temperature influences the amount of air flowing through the boiler because when the temperature is higher, less air is needed because the same amount of energy can go into less air with a higher temperature.

First the start temperature is researched, which shows a parabolic shape when the start and final temperature are plotted against each other in Figure 7.9. The model itself shows to be very influential on the curve, where for *model 1* it would be suggested that a higher start temperature would reduce the eventual end temperature this is not the case for *model 2*. There a lower start temperature would be recommended.
It is also interesting to see that there is a maximum for the curves of both models. The decrease of temperature on the right hand side can be explained by a higher temperature difference between the particles and the wall, so the radiative heat transfer is higher. And by a lower air velocity because less air is needed to contain the energy, so the particles will stay in the boiler longer. The effect on the left hand side is still unknown and possibly because the already low temperature just does not need to cool down that much.

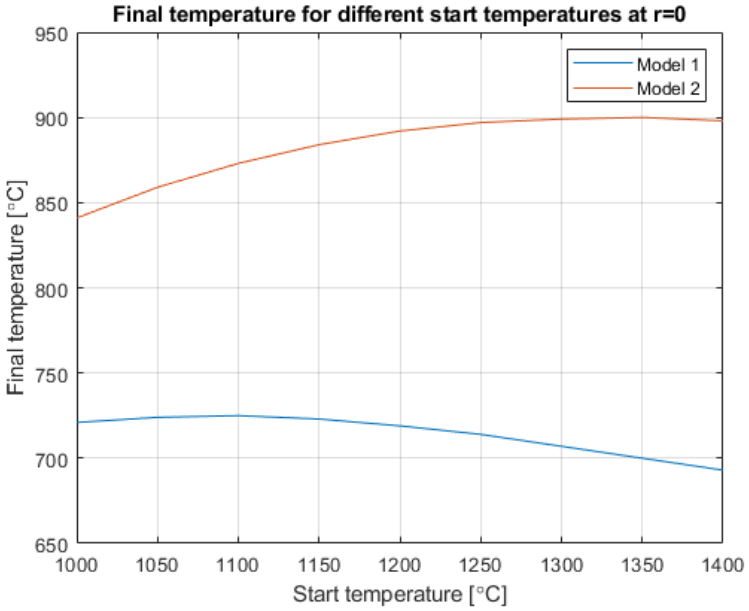

Figure 7.9: The starting temperature and the end temperature plotted against each other.

Next up is the temperature of the wall/steam tubes. It is standard at 180°C so it can not deviate that much compared to the starting temperature. This starting temperature has been set to 1200°C again for this test. It can be seen in Figure 7.10 that adjusting the temperature of the wall has little impact on the end temperature.
Lastly the influence of the input power needs to be determined. In Figure 7.11 it can be seen that for *model 1* a maximum power of 300 kW can be realised and that for *model 2* this is just under 125 kW. Keeping in mind that this is done with the standard values from Table 3, so previously seen optimisations still have to be applied. Further interesting behaviour is that the in Figure 7.11 it seems like the temperature curve will go to a maximum or be hyperbolic. This is interesting because it could mean that for certain design variables final temperature will stay under the design constrain of 800°C for a large power input range. In Figure B.6 it can be seen that for high input power the curve will increase less but it is not the case that a (near) horizontal line is developing for a large input power. Further research is needed to determine if this behaviour could be used to create a better high wattage boiler.

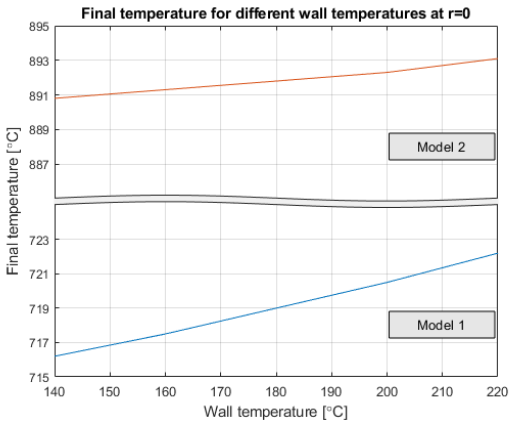

Figure 7.10: Final temperature for different wall /steam tube temperatures.

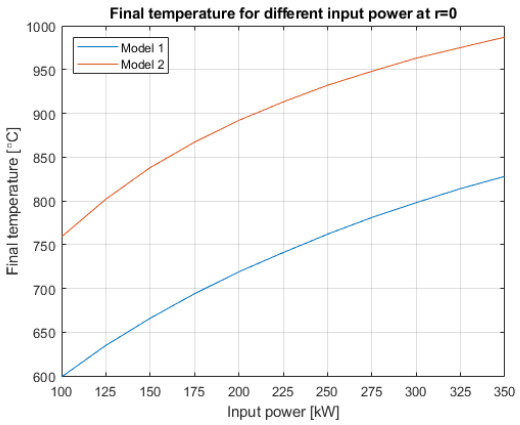

Figure 7.11: Final temperature for different input powers.

7.5 Behaviour of physical variables

For the physical properties of the boiler it is good to realise that between the models there is a mayor difference. Because of the particle tube used in *model 2* it is more difficult to compare with *model 1*. First the radius was adjusted using a range between 0.3 and 0.7 meters. It can be seen in Figure 7.12 that this has mayor influence on the resulting temperature in the case of *model 1*. The end temperature is lower when a larger radius for the pipe is used, one of the likely reasons is the decrease of mean velocity due to the increasing radius. In *model 2* a different trend is shown, because of the difference between the models it results in a temperature increase. This increase is most likely due to a decrease in the view factor while the particles will not be effected by the change in radius.

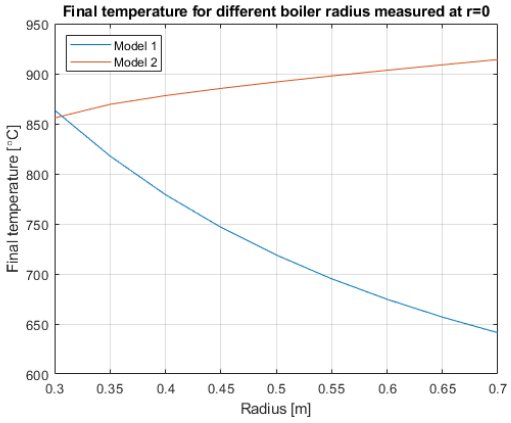

Figure 7.12: Final temperature when the boiler radius is adjusted in *model 1 & 2*.

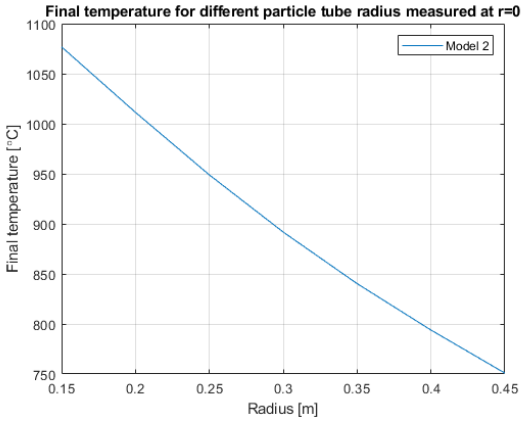

Figure 7.13: Final temperature when only the particle tube radius is adjusted in *model 2*.

For *model 2* it is also interesting to look at the temperature versus the particle tube radius. In Figure 7.13 it shows a massive improvement and with a particle tube radius of 0.4 metres the final temperature constrain of 800°C can be achieved. Changing the particle tube radius is easy to do in a model but on the design this is a fixed value. The boiler will be using a powder burner that has a radius of 0.3525 m. But this burner is also able to make the bring a swirl into the emitted particles, making the air particle mixture rotate inside the boiler around the vertical axis. The centripetal forces will cause the particles to move towards the wall, effectively increasing the particle tube radius. However more research needs to be done to say something concrete about this, the particles have a low weight and have different masses so it is unknown if they are able to move a lot at all and the distribution of particles in the boiler will not be homogeneous anymore, adding complexity to the model.
The length of the boiler is influential as well, in Figure 7.1 and Figure 7.2 it can be seen that the

temperature curve decreases with the length as can be expected. A longer boiler will reduce the temperature more. There is however some interesting behaviour when looking at the length of the boiler. In Figure 7.4 it can be seen that for large particles the temperature will increase when approaching the end of the boiler. This is most likely due to the view factor being lower in that area so the particles can't get their energy to radiate to the wall. The hot air will heat the particles more then the radiation can cool them. Therefore it could be beneficial to also cool the funnel at the bottom of the boiler, so they are also cooled there by an increased view factor.

7.6 Combining Results

With the information above an optimal boiler design can be made. For this an optimal particle distribution, optimal thermal and optimal physical variables should be used. The particle distribution is one of the variables that are uncertain if they can be changed that easily, so it is also necessary to look at the boiler design with the standard distribution that is in Table B.1.

7.6.1 Changing the physical dimensions

The first interesting part is the physical properties of the boiler combined with the model showing in Figure 7.11, where the temperature curve is not linear and that with a higher input power it flattens. Therefore the physical properties have been adjusted, for both models the boiler tube radius has been increased to 0.7 metres and for *model 2* the particle tube radius is also increased to 0.5 metres. In Figure 7.14 the results can be seen. It does hold that the diameter influences this temperature curve the most and that with these values for *model 1* a power input of 250 kW can be realised. Which is a great improvement over the 125 kW of the standard *model 2*. However this is difficult to realise with the set dimensions of the powder burner, but in general a bigger boiler radius is beneficial.
In Figure 7.15 the temperature curve is seen for a boiler with a length of 10 metres. It can be seen that this curve flattens when the boiler becomes longer. But where now the boiler has as constrain it can only be 2.5 metres high a longer boiler tube could be beneficial when that constrain is adjusted. This 10 metre long tube will result in an allowable input power of around 600 kW.

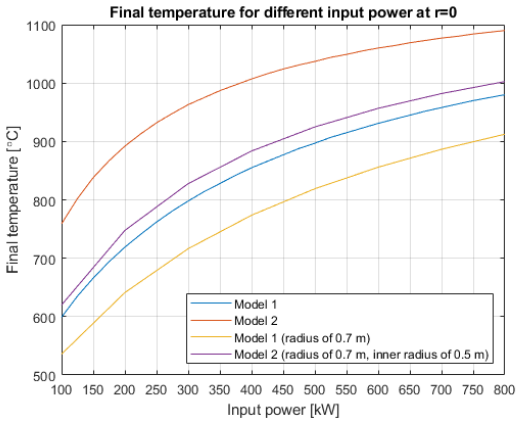

Figure 7.14: Temperature at different power inputs for *model 1* & *model 2* with the boiler tube radius of 0.7 m and for *model 2* the particle tube radius is changed to 0.5.

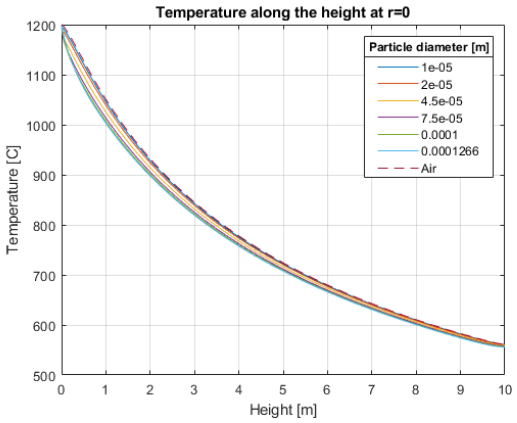

Figure 7.15: Temperature curve of a boiler design with with the standard values from Table 3 with a height of 10 metres using *model 2*.

7.6.2 Changing the particle tube and particle distribution

The particle tube can be changed to a radius of 0.3525 metres because that is the actual radius of the burner. In *model 2* this results in an input power of 160 kW but this could be improved with the use of the swirl, because in Figure 7.13 it shows that if the radius could be increased to a average of 0.4 metres the temperature could allow an input power of 200 kW. However this is still uncertain.
But what can be added to this is a particle distribution that is closer to the optimum. This has been done in Figure 7.16 where it results in a final temperature of 780°C or when the temperature is allowed

to go up to 800°C it will have a input power of 220 kW. Without changing the outer dimensions of the boiler and ignoring the option for a swirl this seems the most effective solution. Trying to decrease the temperature by changing other variables seems to be not worth the trouble, the wall temperature has minor influence on the model and the start temperature can make a difference but it would mean that the temperature needs to change a lot. In Figure 7.17 it can be seen that there is some to gain by increasing the temperature, a 100°C increase in starting temperature would translate into an almost 10°C drop in final temperature. This would mean that the input power can be increased to 225 kW. So this is only a minor increase.

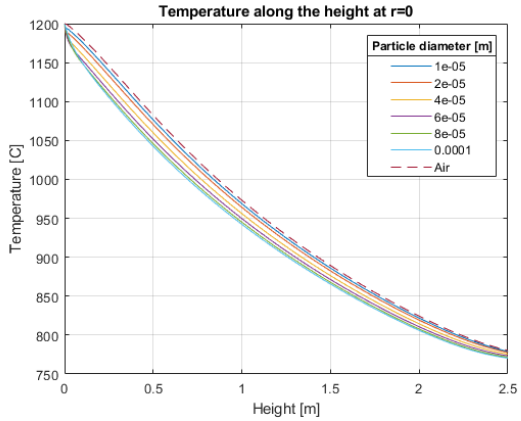

Figure 7.16: Temperature curve along the boiler height in *model 2* with the particle tube radius of 0.3525 m (Table B.3) and a smaller particle distribution (Table B.4).

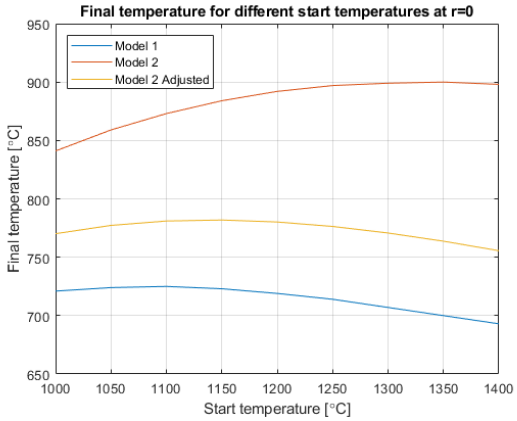

Figure 7.17: The starting temperature and the end temperature plotted against each other for the adjusted *model 2*. Using the variables from Table B.3 but with the starting temperature variable.

7.6.3 Changing all dimensions to create the optimal boiler

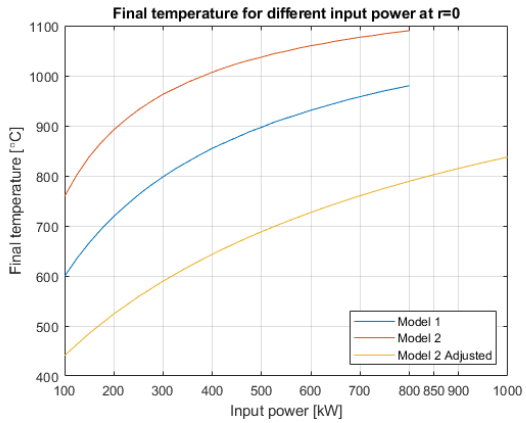

Figure 7.18: Temperature at different power inputs for *model 1*, *model 2* and the adjusted *model 2* with the properties as described in Table B.5 and using the particle distribution in Table B.4.

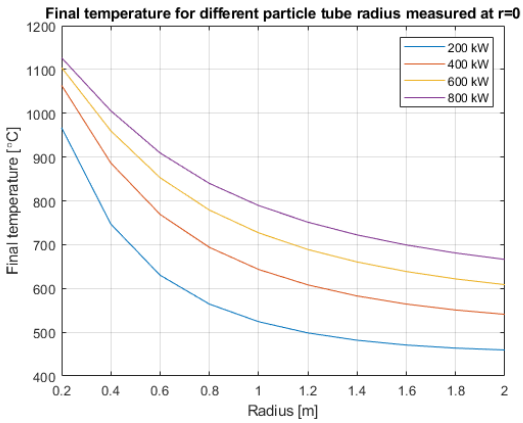

Figure 7.19: Final temperature when the particle tube radius is adjusted in the adjusted *model 2* described in Table B.5, for different power inputs. The outer boiler tube radius is equals to the particle tube radius plus 0.2 m.

The main variable in this part is the outer dimensions of the boiler tube. This can be seen as the most influential parameter because increasing it will always improve the boiler. To create the best boiler design the particle distribution from Figure 7.16 is used in combination increased physical variables. The boiler tube is increased to 1.2 m in size and the particle tube radius is increased to 1.0 m, so the

difference is still 0.2 m. In Figure 7.18 it can be seen that this combination will result in a input power of 840 kW. In Figure 7.19 the final temperature for an increasing boiler and particle tube radius can be seen. This has been done for several power inputs. It can be seen that at a certain radius a further increase will not decrease the temperature a lot, therefore a radius for the particle tube of around 1 metre seems to be optimal. In Table B.5 the variables for this option can be seen.
The wall/steam tube and the starting temperature have not been adjusted. It is possible to get a minor increase in efficiency but as determined before this is only a minor contributor to the overall heat transfer. Therefore they are not adjusted.

However this is not even be the best boiler design possible. With these variables it is interesting too look back at the particle size distribution. In Figure 7.20 the optimal particle size can be determined. It can also be seen that there even seems to be a different optimal particle size when comparing 200 kW and 800 kW. It is interesting to see that when the boiler tube is increased the optimal size becomes larger.
The particle distribution has been changed by filtering out some lower particle sizes as can be seen in Table 4. This reduces the temperature to 781°C when a input power of 840 kW is used. Increasing the input power a maximum of 910 kW can be achieved.

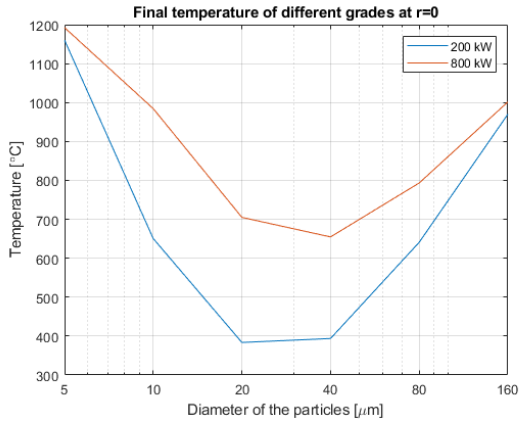

Figure 7.20: Final temperature of mono-disperse grades of the adjusted *model 2* as described by Table B.5, using 200 kW and 800 kW.

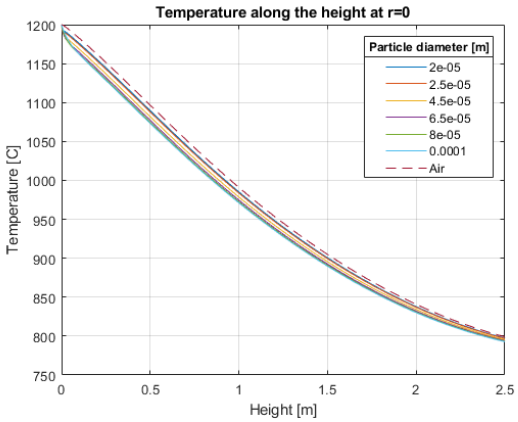

Figure 7.21: Temperature curve of the optimal boiler design described by Table B.5. But using 910 kW instead.

Table 4: Particle distribution optimised for a larger particle tube. (Figure 7.21)

Diameter [μm]	20	25	45	65	80	100
Number fraction [-]	0.0091	0.1062	0.5134	0.2988	0.0620	0.0105

7.6.4 Making the boiler larger

To finalise this thesis a view is given to what is reachable with boilers like this. For this the values from Table B.5 are used except that the boiler has been made 10 metres in height. Also the particle distribution from Table 4 is used. This results in a possible power input of 4.5 MW. So it is possible according to this model to make boilers that are producing in the megawatt range. However do you want to build 1 really big boiler or 11 small ones with the capacity of 220 kW?

8 Conclusion

In short this thesis has given a model and solutions on how to get a boiler design that fits the requirements and constraints set at the start of this project. But there are still questions that should be answered to give a full view on how an once-through metal fuelled boiler works.

8.1 Model

The models made show some clear mechanisms that are important for the boiler. The extinction causes small particles to reduce the view factor, resulting in higher final temperatures for small particles. But on the other hand large particles have a higher terminal velocity and have less efficient heat transfer, causing large particles to increase the final temperature as well. Therefore there is an optimal particle size. When deciding on the particle distribution this optimum should be found first. This optimal particle size is dependent on the properties of the boiler, so boilers with different sizes will also have a different optimal particle size.
Further improvements can be made by using a larger radius for the boiler and having a higher boiler. These variables do have diminishing returns when they are made larger, the curves will flatten as can be seen in Figure 7.12 and Figure 7.15. In this a optimum could be found.
The thermodynamic variables, the starting temperature and the steam tube temperature, are not very effective in influencing the temperatures inside the boiler. The starting temperature shows the most influence in the behaviour of the boiler but is very dependent on the boiler design. Interesting is that it is not clear beforehand if an increase or decrease in starting temperature will result in better boiler behaviour. Depending on the boiler design an increase or decrease will improve the final temperature in the boiler.

8.2 Results

The results show that this type of boiler design has the potential to produce the target power of 200 kW set in this thesis. This can be done using the variables from Table B.3 and a smaller particle distribution in Table B.4. Here the particle tube has the same radius as the powder burner and the distribution is made smaller. This results in a possible power input of 220 kW. Using only the radius of the powder burner would allow an input power of 160 kW.
But interesting is also to see what happens when other variables are adjusted. With adjusting variables like the height and radius it shows that the boiler to reach is full potential. According to the model when using a 10 metre high boiler that has a radius of 1.2 metres and inner particle tube radius of 1 metre a power input of 4.5 MW can be used. This is of course outside the scope of this project but it shows there is potential for this design.

8.3 Improvements

To get to a more accurate model there are several variables that could be included in the model. First there is the problem on the extinction of the radiation. This is now done as described in Equation 4.3 with a extinction efficiency that is set to 2. This however can be looked it to more closely because this is a value that is true when the ratio between the particle diameter and the radiation wavelength is a lot bigger then 1. This ratio is larger for this use case but not by a lot and could use some more research.
A second improvement is the use of a swirl in the powder burner that would let the medium rotate around its vertical axis. This could cause the particles to move towards the outside of the boiler increasing the radius of the particle tube. Therefore improving the efficiency. Problems with this is that the particle distribution will not be homogeneous anymore because larger heavier particles will move to the outside faster then the small ones.

9 Recommendations for the boiler design

This research project is done in cooperation with HeatPower. The goal is to build a once through steam boiler in which iron powder can be burned. There are several requirements preferences and constraints outlined in Table 1 that need to be taken into account. Therefore it is advised to make a boiler with the design described by Figure 7.16. This means that all the values from Table B.3 are used together with the distribution from Table B.4. A boiler with these variables will be able to burn 220 kW of iron and in that case the maximum final temperature at the bottom of the boiler will be 800°C. All variables concerning the boiler design can be found in Table 5.

Table 5: Recommended boiler design variables.

Boiler height	2.5 m
Boiler wall diameter	1.0 m
Steam tube temperature	180°C
Particle tube diameter	0.705 m
Starting temperature	1200°C

With these variables it does not mean that everything is set yet. The powder burner also has the possibility to make the medium swirl. In theory this could cause the particles to move towards the wall of the boiler increasing the diameter of the particle tube and increasing the efficiency of the boiler. This is not modelled into the model but could still be experimented with when the boiler is build.

References

Ahmed, S. N. (2015). *Physics and engineering of radiation detection* (Second ed.). Amsterdam, Netherlands: Elsevier. Retrieved from https://www.sciencedirect.com/science/book/9780128013632

Bergthorson, J. M., Goroshin, S., Soo, M. J., Julien, P., Palecka, J., Frost, D. L., & Jarvis, D. J. (2015). Direct combustion of recyclable metal fuels for zero-carbon heat and power. *Applied Energy*, *160*, 368–382. doi: 10.1016/j.apenergy.2015.09.037

Butcher, J. C. J. C. (2016). *Numerical methods for ordinary differential equations* (Third ed.). Chichester, UK: Wiley. Retrieved from http://www.myilibrary.com?id=940957

Diepstraten, L. (2021). *Preliminary design of a once-through boiler for a metal fuel burner* (Bachelor's Thesis). Eindhoven University of Technology.

Modest, M. F. (2013). *Radiative heat transfer* (Third ed.). San Diego: Elsevier Science. Retrieved from https://www.sciencedirect.com/science/book/9780123869449

van Leeuwen, M. (2021). *Modelling the heat transfer of a once-through boiler for a metal fuel burner* (Bachelor's Thesis). Eindhoven University of Technology.

Welty, J. R., Rorrer, G. L., & Foster, D. G. (2015). *Fundmentals of Momentum, Heat and Mass Transfer* (sixth ed.). Singapore: John Wiley & Sons.

Whitaker, S. (1972). Forced convection heat transfer correlations for flow in pipes, past flat plates, single cylinders, single spheres, and for flow in packed beds and tube bundles. *AIChE Journal*, *18*(2), 361–371. Retrieved from https://aiche.onlinelibrary.wiley.com/doi/abs/10.1002/aic.690180219 doi: https://doi.org/10.1002/aic.690180219

Young, R. M., & Pfender, E. (1987). Nusselt number correlations for heat transfer to small spheres in thermal plasma flows. *Plasma Chemistry and Plasma Processing*, *7*(2), 211–229. doi: 10.1007/BF01019179LK-https://tue.on.worldcat.org/oclc/5656067415

Yow, H. N., Pitt, M. J., & Salman, A. D. (2005). Drag correlations for particles of regular shape. *Advanced Powder Technology*, *16*(4), 363–372.

A Matlab models

A.1 *Model 1*: Fully distributed over the boiler tube

```
clear all; close all;

%% Constants
% Geometric properties
Watt        =    330 * 10^3;                          %Energy input [W]
H_v         =    5.2e6;                               %Heating value iron [J/kg]
T_iron      =    1200 + 273;                          %Start temperature iron particles [K]
M_iron      =    Watt/H_v;                            %total iron massflow [kg/s]
T_pipe      =    180 + 273;                           %Start temperature pipe [K]
r_p         =    0.5;                                 %Radius of the tube [m]
L_p         =    2.5;                                 %Length of the tube [m]

% Media properties
Cp_Air      =    1154;%1134;                          %Specific heat Air [J/kg K]
Rho_Air     =    0.369217;                            %Density Air at film temperature [kg/m3]
Mu_Air      =    4.332e-5;%4.0549275 * 10^-5;         %Viscosity air [Pa s]
k_Air       =    7.135e-2;%6.573 * 10^-2;             %Thermal conductivity air [W/(m K)]

Cp_Fe2O3    =    654;                                 %Specific heat iron oxide particles [J/kg K]
Rho_Fe      =    7860;                                %Density iron [kg/m3]
Rho_Fe2O3   =    5242;                                %Density ironoxide [kg/m3]

% Transfer properties
sigma       =    5.67 * 10^-8;                        %Stefan-Boltzmann constant [J/ (m^2 s K^4)]
e_1         =    0.85;                                %Emissivity of the the iron particle [-]

% Derived variables
M_oxide     =  M_iron*Rho_Fe2O3/Rho_Fe;               %Massflow oxide particles [kg/s]
M_flow_Air  = (Watt-M_oxide*Cp_Fe2O3*(T_iron-293))/...
                (Cp_Air *(T_iron-293));               %Mass flow Air [kg/s]
A_c         =  pi * r_p.^2;                           %Surface cross section pipe [m2]
v_mean      =  M_flow_Air ./ (Rho_Air .* A_c);        %Mean velocity at beginning of tube [m/s]


% Particle distribution

filename={'Ferchim MT 63-3_4.txt'};
for i=1:length(filename)
    Data{i}=readtable(filename{i});
end
MT63 = table2array(Data{1});
for i=1:100
    if MT63(101-i,2) == 0
       MT63(101-i,:) = [];
    end
end
MT63(:,3) = [];
MT63(:,1) = (MT63(:,1)/2)*10^(-6);
MT63(:,2) = MT63(:,2)*10^(-2);
riNi = transpose(MT63);

%riNi = [(10-0)*1e-6/2 (20)*1e-6/2 (45)*1e-6/2 (75)*1e-6/2 (100)*1e-6/2 (126.6)*1e-6/2;
%        .0091 .1062 .5134 .2988 .062 .0105];
%riNi = [18e-6/2; 1];
kmax = size(riNi,2);

for k=1:kmax
    r_Fe2O3(k) =    riNi(1,k);                        %Radius of the iron oxide particle [m]
    A_iron(k)  =    4*pi*r_Fe2O3(k)^2;                %surface iron particle [m^2]
    M_Fe2O3(k) =    4/3*pi*Rho_Fe2O3*r_Fe2O3(k)^3;    %Mass ironoxide particle [kg]
end

% Nusselt number                                      %Nusselt for particle/gas heat transfer
syms V
for k=1:kmax
    C_D(k) = (23.5/((2*r_Fe2O3(k)*Rho_Air*V)/Mu_Air) + 4.6./sqrt((2*r_Fe2O3(k)*Rho_Air*V)/Mu_Air)+ 0.3);
    eqn = C_D(k)*V^2 == (4*Rho_Fe2O3*2*r_Fe2O3(k)*9.81)/(3*Rho_Air);

    % eqn = (V.^2)*A_iron(k)*(23.5/((2*r_Fe2O3(k)*Rho_Air*V)/Mu_Air)...
    %         + 4.6./sqrt((2*r_Fe2O3(k)*Rho_Air*V)/Mu_Air)+ 0.3) == (8*9.81*M_Fe2O3(k))/Rho_Air;
    v_infty(k) =  vpasolve(eqn,V,[0,10]);
end
v_infty = double(v_infty);                            %Terminal velocity [m/s]
Re_D = (2*r_Fe2O3.*v_infty.*Rho_Air)/Mu_Air;          %Reynolds number
Nuss = 2+(0.6*(((Mu_Air*Cp_Air)/k_Air)^(1/3)).*(Re_D.^(1/2)));   %Nusselt number


% Extinction coefficient
n_part  = riNi(2,:).*M_Fe2O3/sum(riNi(2,:).*M_Fe2O3)*M_oxide./...
```

```
            (A_c.*(v_mean + v_infty).*M_Fe2O3);                    %Particles per m^3
wtot     = sum(n_part.*(riNi(1,:).^3).*(4/3).*pi*Rho_Fe2O3);       %total weight in particle distribution
Qext     = 2;                                                      %Extinction efficiency
for i=1:kmax
    mu_i(i) = sum(n_part)*(riNi(1,i)^2)*pi*Qext;                   %extinction coefficient per particle
    w_i(i) = (n_part(i).*(riNi(1,i)^3)*(4/3)*pi*Rho_Fe2O3)./wtot;  %weight fraction per particle
end
mu_t = sum(mu_i.*w_i);                                             %extinction coefficient

% Discritisation properties
Nv=41;dr=r_p/(Nv-1);dr2=dr*dr;
Npipe=801;dh=L_p/(Npipe-1);


%% Matrix initialisation
va=v_mean*ones(Nv,Npipe);va(Nv,1:Npipe)=0;
Ta=T_iron*ones(Nv,Npipe);Ta(Nv,1:Npipe)=T_pipe;
Tp=T_iron*ones(kmax,Nv,Npipe);
Qdot=zeros(k,Nv,Npipe);
F12=zeros(Nv,Npipe);

for j=2:Npipe
    L=(j-1)*dh;
    Mflow=0;
    for i=1:Nv-1
        r=(i-1)*dr;

        % Viewfactor & Extinction for L and r
        Rr  = @(phi) r.*cos(phi)+sqrt(r_p^2-(r.*sin(phi)).^2);          %Length to the wall
        fun = @(phi,h) (Rr(phi).^2*r_p)./(pi*(Rr(phi).^2+h.^2).^2)...  %Viewfactor times...
              .*exp(-mu_t*sqrt(Rr(phi).^2+h.^2));                      %...the extinction
        F12(i,j) = (integral2(fun,0,2*pi,L-L_p,L,'AbsTol',1e-3)/pi);   %Viewfactor integral


        % Particle heat transfer
        Qexhtot=0;
        for k=1:kmax
           % Radiation heat transfer per particle
           Qdot(k,i,j)  = sigma * A_iron(k)*(Tp(k,i,j-1)^4 - T_pipe^4)/(1/e_1 -1 +1/F12(i,j));

           %particle Temperature with radiation (Qdot) and convection. Particle speed equals va + v_infty
           Tp(k,i,j)    = (Tp(k,i,j-1)-(Qdot(k,i,j)-Nuss(k)*k_Air*2*pi*r_Fe2O3(k)*Ta(i,j-1))*dh/...
                          (Cp_Fe2O3*M_Fe2O3(k)*(va(i,j-1)+v_infty(k))))/...
                          (1+Nuss(k)*k_Air*2*pi*r_Fe2O3(k)*dh/...
                          (Cp_Fe2O3*M_Fe2O3(k)*(va(i,j-1)+v_infty(k))));

           % Heat transfer for part/gas using Re_D
           Qexh         = Nuss(k)*k_Air*2*pi*r_Fe2O3(k)*(Tp(k,i,j)-Ta(i,j-1));
           Qexhtot      = Qexhtot+n_part(k)*Qexh;
        end

        % Fluid heattransfer : conv/cond 2D x,y (simplified to Cartesian
        % since R >> boundary layer thickness)+ heat through part/gas
        % transfer
        if i==1
           dv=Mu_Air*(2*va(i+1,j-1)-2*va(i,j-1))/dr2;
           dT= k_Air*(2*Ta(i+1,j-1)-2*Ta(i,j-1))/dr2+Qexhtot;
        else
           dv=Mu_Air*(va(i+1,j-1)-2*va(i,j-1)+va(i-1,j-1))/dr2;
           dT= k_Air*(Ta(i+1,j-1)-2*Ta(i,j-1)+Ta(i-1,j-1))/dr2+Qexhtot;
        end

        % Correcting velocity profile for mass conservation (no inertia or
        % pressure gradient is taken into account)
        Rho=Rho_Air*T_iron/Ta(i,j-1);
        va(i,j)=va(i,j-1)+dh*dv/(Rho*va(i,j-1));
        Ta(i,j)=max(T_pipe,Ta(i,j-1)+dh*dT/(Rho*Cp_Air*va(i,j-1)));
        Mflow=Mflow+Rho*va(i,j)*2*pi*r*dr;
    end
    va(:,j)=va(:,j)*M_flow_Air/Mflow;
end

% Calculating total heat transfer (enthaply release of fluid and particles)
for i=1:Nv
    r=(i-1)*dr;
    xx(i,1:Npipe)=(i-1)*dr;
    Rho=Rho_Air*T_iron/Ta(i,Npipe);
    Qtot(i)=Rho*Cp_Air*va(i,Npipe)*(T_iron-Ta(i,Npipe))*2*pi*r*dr;
    for k=1:kmax
        Qtot(i)=Qtot(i)+ ...
            M_Fe2O3(k)*n_part(k)*Cp_Fe2O3*va(i,Npipe)*(T_iron-Tp(k,i,Npipe))*2*pi*r*dr;
    end
end

% Estimate heat transfer through conduction at wall
```

```
for j=1:Npipe
     Qconv(j)=k_Air*(Ta(Nv-1,j)-T_pipe)*dh*2*pi*r_p/dr;
     LL(1:Nv,j)=4-(j-1)*dh;
end

%% Final results
Q_tot       =    sum(Qtot)
Q_conv      =    sum(Qconv)
Q_rad       =    Q_tot-Q_conv
T_end       =    Ta(:,end)-273;                    %End temperature [K]

%% Figures
colormap('jet')

figure(1)
    pcolor(xx,LL,F12)
    title('Viewfactor')
    xlabel('Width [m]')
    ylabel('Length [m]')
    shading('interp')
    colorbar('vert')
    axis('image')

figure(2)
    for p=1:kmax
        subplot(1,kmax,p)
        Ppp(:,:)=Tp(p,:,:);
        pcolor(xx,LL,Ppp-273)
        title(['Particle Temp [C], r_{i} = ', num2str(riNi(1,p)), ' [m]'])
        xlabel('Width [m]')
        ylabel('Length [m]')
        shading('interp')
        axis('image')
    end
hp4 = get(subplot(1,kmax,kmax),'Position');
colorbar('Position', [hp4(1)+hp4(3)  hp4(2)  .01  hp4(4)])

figure(3)
    subplot(1,2,1)
    Ppp(:,:)=Qdot(1,:,:);
    pcolor(xx,LL,Ppp)
    title('Heat transfer [W]')
    xlabel('Width [m]')
    ylabel('Length [m]')
    shading('interp')
    colorbar('vert')
    axis('image')

    subplot(1,2,2)
    Ppp(:,:)=Qdot(2,:,:);
    pcolor(xx,LL,Ppp)
    title('Heat transfer [W]')
    xlabel('Width [m]')
    ylabel('Length [m]')
    shading('interp')
    colorbar('vert')
    axis('image')

figure(4)
    subplot(1,2,1)
    pcolor(xx,LL,va)
    colorbar('vert')
    axis('image')
    shading('interp')

    subplot(1,2,2)
    pcolor(xx,LL,Ta-273)
    colorbar('vert')
    axis('image')
    shading('interp')

figure(5)
    for k=1:kmax
        plot(xx(1:Nv-1,1),Tp(k,1:Nv-1,Npipe)-273)
        hold on
    end
    plot(xx(1:Nv-1,1),Ta(1:Nv-1,Npipe)-273,'--')
    legend(num2str(riNi(1,1)),num2str(riNi(1,2)),num2str(riNi(1,3))...
        ,num2str(riNi(1,4)),num2str(riNi(1,5)),num2str(riNi(1,6)),'Air')
    title('Temperature of the cross section at L=0')
    grid on
    xlabel('Radius [m]')
    ylabel('Temperature [C]')

figure(6)
```

```
    for k=1:kmax
        Ppp=Tp(k,1,:);
        plot(4-LL(1,:),Ppp(:)-273)
        hold on
    end
    plot(4-LL(1,:),Ta(1,:)-273,'--')
    legend(num2str(riNi(1,1)),num2str(riNi(1,2)),num2str(riNi(1,3))...
        ,num2str(riNi(1,4)),num2str(riNi(1,5)),num2str(riNi(1,6)),'Air');
    title('Temperature along the height at r=0')
    grid on
    ylabel('Temperature [\circC]')
    xlabel('Height [m]')
```

A.2 *Model 2*: Centrally distributed in the middle of the boiler tube

```
clear all; close all;

%% Constants
% Geometric properties
Watt        =    200 * 10^3;                    %Energy input [W]
H_v         =    5.2e6;                         %Heating value iron [J/kg]
T_iron      =    1200 + 273;                    %Start temperature iron particles [K]
M_iron      =    Watt/H_v;                      %total iron massflow [kg/s]
T_pipe      =    180 + 273;                     %Start temperature pipe [K]
r_p         =    0.40;                          %Radius of the tube [m]
L_p         =    2.5;                           %Length of the tube [m]
r_p2        =    0.5;                           %Radius of the particle tube [m]

% Media properties
Cp_Air      =    1134;                          %Specific heat Air [J/kg K]
Rho_Air     =    0.369217;                      %Density Air at film temperature [kg/m3]
Mu_Air      =    4.0549275 * 10^-5;             %Viscosity air [Pa s]
k_Air       =    6.573 * 10^-2;                 %Thermal conductivity air [W/(m K)]

Cp_Fe2O3    =    654;                           %Specific heat iron oxide particles [J/kg K]
Rho_Fe      =    7860;                          %Density iron [kg/m3]
Rho_Fe2O3   =    5242;                          %Density ironoxide [kg/m3]

% Transfer properties
sigma       =    5.67 * 10^-8;                  %Stefan-Boltzmann constant [J/ (m^2 s K^4)]
e_1         =    0.85;                          %Emissivity of the the iron particle [-]

% Derived variables
M_oxide     =  M_iron*Rho_Fe2O3/Rho_Fe;         %Massflow oxide particles [kg/s]
M_flow_Air  =  (Watt-M_oxide*Cp_Fe2O3*(T_iron-293))/...
                (Cp_Air *(T_iron-293));         %Mass flow Air [kg/s]
A_c         =  pi * r_p2.^2;                    %Surface cross section pipe [m2]
A_p         =  pi*r_p.^2;                       %Surface cross section particle tube [m2]
v_mean      =  M_flow_Air ./ (Rho_Air .* A_p);  %Mean velocity at beginning of tube [m/s]


% Particle distribution

filename={'Ferchim MT 63-3_4.txt'};
for i=1:length(filename)
    Data{i}=readtable(filename{i});
end
MT63 = table2array(Data{1});
for i=1:100
    if MT63(101-i,2) == 0
       MT63(101-i,:) = [];
    end
end
MT63(:,3) = [];
MT63(:,1) = (MT63(:,1)/2)*10^(-6);
MT63(:,2) = MT63(:,2)*10^(-2);
riNi = transpose(MT63);

riNi = [(10-0)*1e-6/2 (20-0)*1e-6/2 (45-0)*1e-6/2 (75-0)*1e-6/2 (100-0)*1e-6/2 (126.6-0)*1e-6/2;...
        .0091 .1062 .5134 .2988 .062 .0105];
%riNi = [126.6e-6/2; 1];
kmax = size(riNi,2);

for k=1:kmax
    r_Fe2O3(k) =    riNi(1,k);                  %Radius of the iron oxide particle [m]
    A_iron(k)  =    4*pi*r_Fe2O3(k)^2;          %surface iron particle [m^2]
    M_Fe2O3(k) =    4/3*pi*Rho_Fe2O3*r_Fe2O3(k)^3;  %Mass ironoxide particle [kg]
end

% Nusselt number                                %Nusselt for particle/gas heat transfer
syms V
for k=1:kmax
```

```
C_D(k) = (23.5/((2*r_Fe2O3(k)*Rho_Air*V)/Mu_Air) + 4.6./sqrt((2*r_Fe2O3(k)*Rho_Air*V)/Mu_Air)+ 0.3);
eqn = C_D(k)*V^2 == (4*Rho_Fe2O3*2*r_Fe2O3(k)*9.81)/(3*Rho_Air);

%eqn = (V.^2)*A_iron(k)*(23.5/((2*r_Fe2O3(k)*Rho_Air*V)/Mu_Air)...
%        + 4.6./sqrt((2*r_Fe2O3(k)*Rho_Air*V)/Mu_Air)+ 0.3) == (8*9.81*M_Fe2O3(k))/Rho_Air;
v_infty(k) =  vpasolve(eqn,V,[0,10]);
end

v_infty = double(v_infty);                                          %Terminal velocity
Re_D = (2*r_Fe2O3.*v_infty.*Rho_Air)/Mu_Air;                        %Reynolds number
Nuss = 2+(0.6*(((Mu_Air*Cp_Air)/k_Air).^(1/3)).*(Re_D.^(1/2)));     %Nusselt number

% Extinction coefficient
n_part  = riNi(2,:).*M_Fe2O3/sum(riNi(2,:).*M_Fe2O3)*M_oxide./...
            (A_p.*(v_mean + v_infty).*M_Fe2O3);                     %Particles per m^3
wtot    = sum(n_part.*(riNi(1,:).^3).*(4/3).*pi*Rho_Fe2O3);         %total weight in particle distribution
Qext    = 2;                                                        %Extinction efficiency
for i=1:kmax
    mu_i(i) = sum(n_part)*(riNi(1,i).^2)*pi*Qext;                   %extinction coefficient per particle
    w_i(i) = (n_part(i).*(riNi(1,i).^3)*(4/3)*pi*Rho_Fe2O3)./wtot;  %weight fraction per particle
end
mu_t = sum(mu_i.*w_i);                                              %extinction coefficient

% Discritisation properties
Nv=41;dr=r_p/(Nv-1);dr2=dr*dr;
Npipe=801;dh=L_p/(Npipe-1);


%% Matrix initialisation
va=v_mean*ones(Nv,Npipe);va(Nv,1:Npipe)=0;
Ta=T_iron*ones(Nv,Npipe);Ta(Nv,1:Npipe)=T_pipe;
Tp=T_iron*ones(kmax,Nv,Npipe);
Qdot=zeros(k,Nv,Npipe);
F12=zeros(Nv,Npipe);

for j=2:Npipe
    L=(j-1)*dh;
    Mflow=0;
    for i=1:Nv-1
        r=(i-1)*dr;

        % Viewfactor & Extinction for L and r
        Rr  = @(phi) r.*cos(phi)+sqrt(r_p^2-(r.*sin(phi)).^2);          %Length to the wall
        Rr2 = @(phi) r.*cos(phi)+sqrt(r_p2^2-(r.*sin(phi)).^2);         %Length though particle tube
        fun = @(phi,h) (Rr2(phi).^2*r_p2)./(pi*(Rr2(phi).^2+h.^2).^2)... %Viewfactor times...
            .*exp(-mu_t*sqrt(Rr(phi).^2+h.^2));                         %...the extinction
        F12(i,j) = (integral2(fun,0,2*pi,L-L_p,L,'AbsTol',1e-3)/pi);    %Viewfactor integral


        % Particle heat transfer
        Qexhtot=0;
        for k=1:kmax
            % Radiation heat transfer per particle
            Qdot(k,i,j) = sigma * A_iron(k)*(Tp(k,i,j-1)^4 - T_pipe^4)/(1/e_1 -1 +1/F12(i,j));

            %particle Temperature with radiation (Qdot) and convection. Particle speed equals va + v_infty
            Tp(k,i,j)   = (Tp(k,i,j-1)-(Qdot(k,i,j)-Nuss(k)*k_Air*2*pi*r_Fe2O3(k)*Ta(i,j-1))*dh/...
                           (Cp_Fe2O3*M_Fe2O3(k)*(va(i,j-1)+v_infty(k))))/...
                           (1+Nuss(k)*k_Air*2*pi*r_Fe2O3(k)*dh/...
                           (Cp_Fe2O3*M_Fe2O3(k)*(va(i,j-1)+v_infty(k))));

            % Heat transfer for part/gas using Re_D
            Qexh        = Nuss(k)*k_Air*2*pi*r_Fe2O3(k)*(Tp(k,i,j)-Ta(i,j-1));
            Qexhtot     = Qexhtot+n_part(k)*Qexh;
        end

        %No convective heat transfer with the wall.

        % Correcting velocity profile for mass conservation (no inertia or
        % pressure gradient is taken into account)
        Rho=Rho_Air*T_iron/Ta(i,j-1);
        va(i,j)=va(i,j-1);
        Ta(i,j)=max(T_pipe,Ta(i,j-1)+dh*Qexhtot/(Rho*Cp_Air*va(i,j-1)));
        Mflow=Mflow+Rho*va(i,j)*2*pi*r*dr;
    end
    va(:,j)=va(:,j)*M_flow_Air/Mflow;
end

% Calculating total heat transfer (enthaply release of fluid and particles)
for i=1:Nv
    r=(i-1)*dr;
    xx(i,1:Npipe)=(i-1)*dr;
    Rho=Rho_Air*T_iron/Ta(i,Npipe);
    Qtot(i)=Rho*Cp_Air*va(i,Npipe)*(T_iron-Ta(i,Npipe))*2*pi*r*dr;
    for k=1:kmax
```

```
153             Qtot(i)=Qtot(i)+ ...
154                 M_Fe2O3(k)*n_part(k)*Cp_Fe2O3*va(i,Npipe)*(T_iron-Tp(k,i,Npipe))*2*pi*r*dr;
155         end
156 end
157
158 % Estimate heat transfer through conduction at wall
159 for j=1:Npipe
160         Qconv(j)=k_Air*(Ta(Nv-1,j)-T_pipe)*dh*2*pi*r_p/dr;
161         LL(1:Nv,j)=4-(j-1)*dh;
162 end
163
164 %% Final results
165 Q_tot           =       sum(Qtot)
166 Q_conv          =       sum(Qconv)
167 Q_rad           =       Q_tot-Q_conv
168 T_end           =       Ta(:,end)-273;                          %End temperature [K]
169
170 %% Figures
171 colormap('jet')
172
173 figure(1)
174     pcolor(xx,LL,F12)
175     title('Viewfactor')
176     xlabel('Width [m]')
177     ylabel('Length [m]')
178     shading('interp')
179     colorbar('vert')
180     axis('image')
181
182 figure(2)
183     for p=1:kmax
184         subplot(1,kmax,p)
185         Ppp(:,:)=Tp(p,:,:);
186         pcolor(xx,LL,Ppp-273)
187         title(['Particle Temp [C], r_{i} = ', num2str(riNi(1,p)), ' [m]'])
188         xlabel('Width [m]')
189         ylabel('Length [m]')
190         shading('interp')
191         axis('image')
192     end
193     hp4 = get(subplot(1,kmax,kmax),'Position');
194     colorbar('Position', [hp4(1)+hp4(3)  hp4(2)  .01  hp4(4)])
195
196 figure(3)
197     subplot(1,2,1)
198     Ppp(:,:)=Qdot(1,:,:);
199     pcolor(xx,LL,Ppp)
200     title('Heat transfer [W]')
201     xlabel('Width [m]')
202     ylabel('Length [m]')
203     shading('interp')
204     colorbar('vert')
205     axis('image')
206
207     subplot(1,2,2)
208     Ppp(:,:)=Qdot(2,:,:);
209     pcolor(xx,LL,Ppp)
210     title('Heat transfer [W]')
211     xlabel('Width [m]')
212     ylabel('Length [m]')
213     shading('interp')
214     colorbar('vert')
215     axis('image')
216
217 figure(4)
218     subplot(1,2,1)
219     pcolor(xx,LL,va)
220     colorbar('vert')
221     axis('image')
222     shading('interp')
223
224     subplot(1,2,2)
225     pcolor(xx,LL,Ta-273)
226     colorbar('vert')
227     axis('image')
228     shading('interp')
229
230 figure(5)
231     for k=1:kmax
232         plot(xx(1:Nv-1,1),Tp(k,1:Nv-1,Npipe)-273)
233         hold on
234     end
235     plot(xx(1:Nv-1,1),Ta(1:Nv-1,Npipe)-273,'--')
236     legend(num2str(riNi(1,1)),num2str(riNi(1,2)),num2str(riNi(1,3))...
237         ,num2str(riNi(1,4)),num2str(riNi(1,5)),num2str(riNi(1,6)),'Air')
```

```
238     title('Temperature of the cross section at L=0')
239     grid on
240     xlabel('Radius [m]')
241     ylabel('Temperature [C]')
242
243 figure(6)
244     for k=1:kmax
245         Ppp=Tp(k,1,:);
246         plot(4-LL(1,:),Ppp(:)-273)
247         hold on
248     end
249     plot(4-LL(1,:),Ta(1,:)-273,'--')
250     legend(num2str(riNi(1,1)),num2str(riNi(1,2)),num2str(riNi(1,3))...
251         ,num2str(riNi(1,4)),num2str(riNi(1,5)),num2str(riNi(1,6)),'Air');
252     title('Temperature along the height at r=0')
253     grid on
254     ylabel('Temperature [C]')
255     xlabel('Height [m]')
```

A.3 Graphs showing the sensitivity of the models

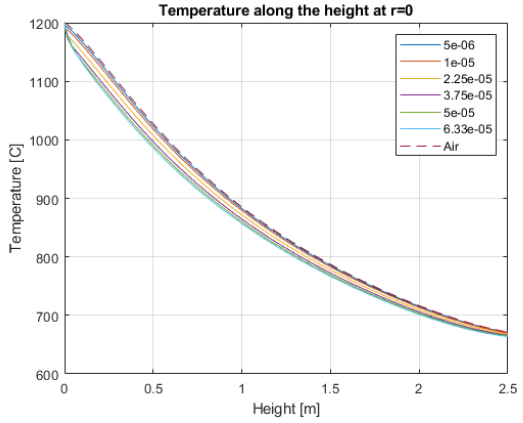

Figure A.1: Temperature with the lowest possible air properties for *model 1*.

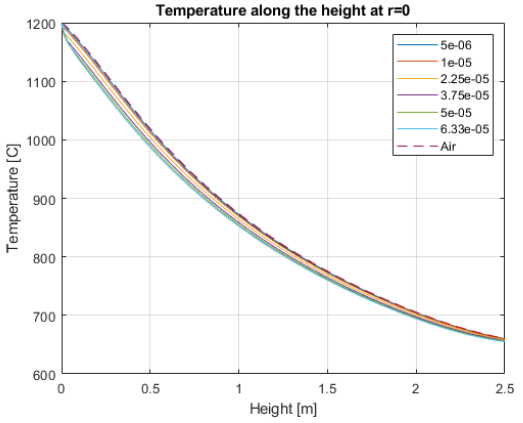

Figure A.2: Temperature with the highest possible air properties for *model 1*.

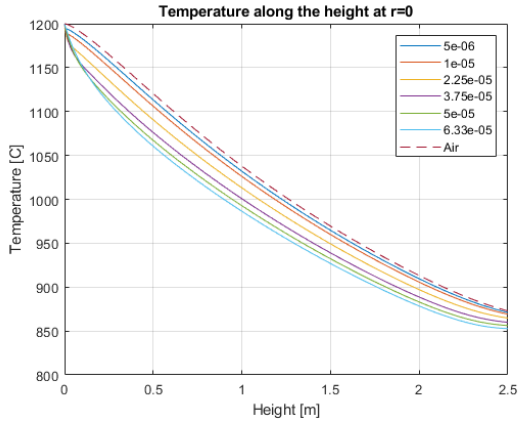

Figure A.3: Temperature with the lowest possible air properties for *model 2*.

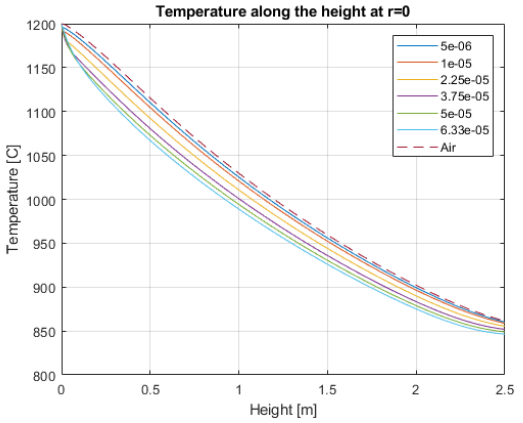

Figure A.4: Temperature with the highest possible air properties for *model 2*.

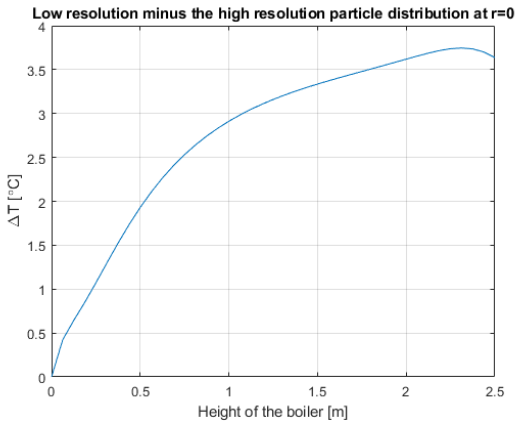

Figure A.5: Temperature difference (ΔT) where the low resolution is compared to the high resolution along the height of the boiler. The measurement is done in the centre of the boiler so where the radius is zero. (*model 2*)

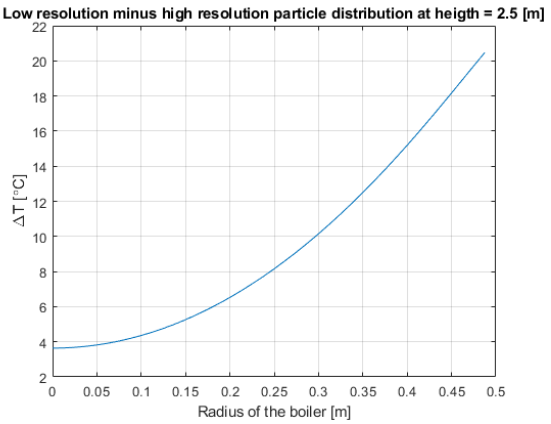

Figure A.6: Temperature difference (ΔT) where the low resolution is compared to the high resolution along the radius of the boiler. The measurement is done at the end/bottom of the boiler so where the height is defined as 2.5 [m]. (*model 2*)

B Results from the model

In this appendix figures and tables are presented that are give a result from the model or are used in the model.

(a) *model 1* (b) *model 2*

Figure B.1: View factor of both models using the standard values in Table 3.

Table B.1: Low resolution particle distribution.

Diameter [μm]	10	20	45	75	100	126.6
Number fraction [-]	0.0091	0.1062	0.5134	0.2988	0.0620	0.0105

Table B.2: Particle distribution from a high resolution used to get accurate values.

Particle diameter [μm]	5.916	6.721	7.636	8.676	9.858	11.20	12.72	14.45	16.42
Number fraction [-]	0.0004	0.0009	0.0013	0.0022	0.0038	0.0061	0.0096	0.0149	0.0220
Particle diameter [μm]	18.66	21.20	24.09	27.37	31.10	35.33	40.14	45.61	51.82
Number fraction [-]	0.0321	0.0444	0.0584	0.0719	0.0837	0.0922	0.0971	0.0975	0.0925
Particle diameter [μm]	58.87	66.89	76.00	86.35	98.11	111.4	126.6		
Number fraction [-]	0.082	0.0675	0.0506	0.0352	0.0217	0.0098	0.0022		

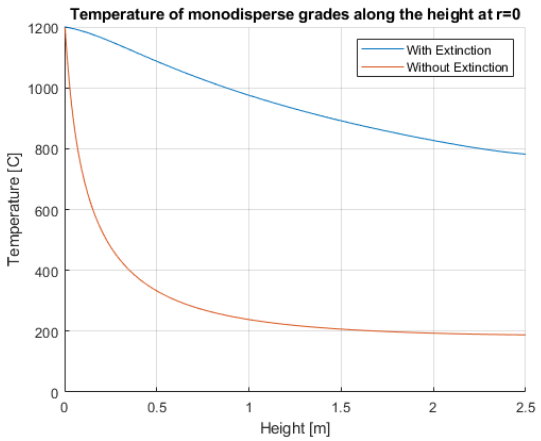

(a) Particle with a diameter of 5 μm.

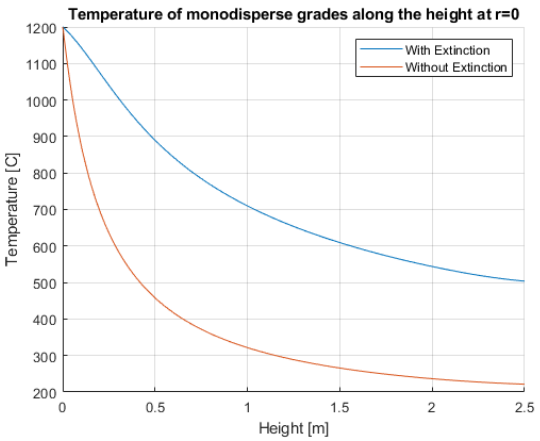

(b) Particle with a diameter of 10 μm.

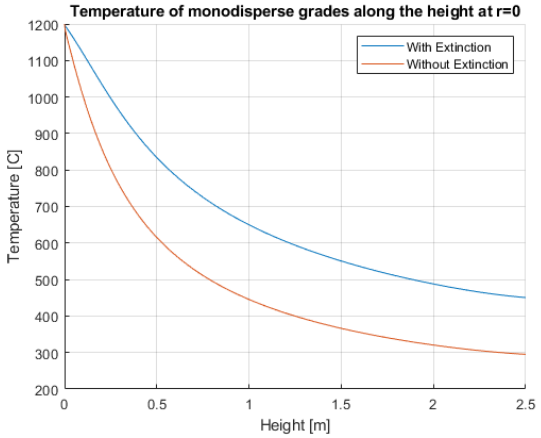

(c) Particle with a diameter of 20 μm.

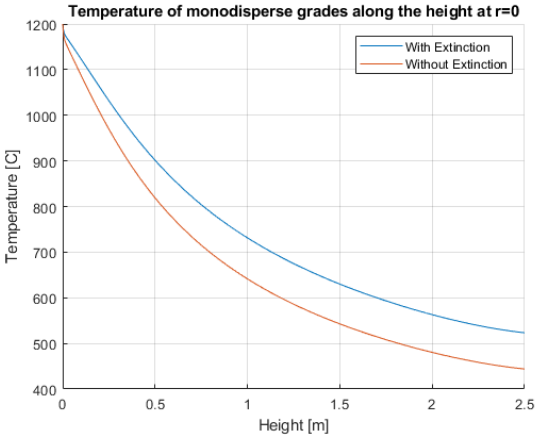

(d) Particle with a diameter of 45 μm.

Figure B.2: Temperature of the mono-disperse grade where the extinction is taken out.

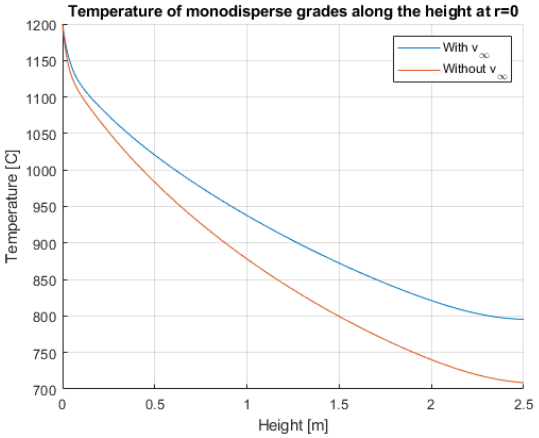

(a) Particle with a diameter of 126.6 μm.

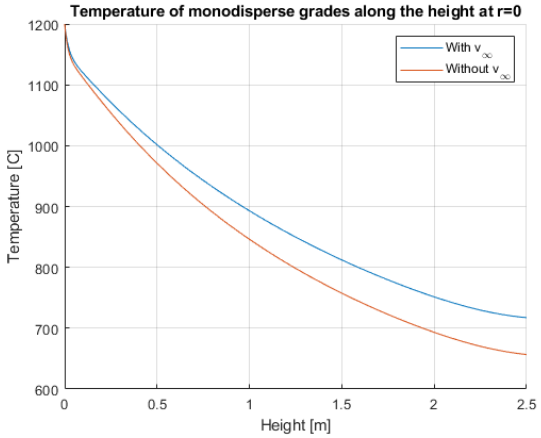

(b) Particle with a diameter of 100 μm.

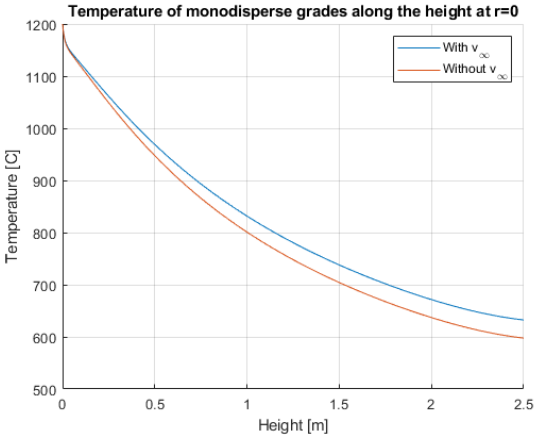

(c) Particle with a diameter of 75 μm.

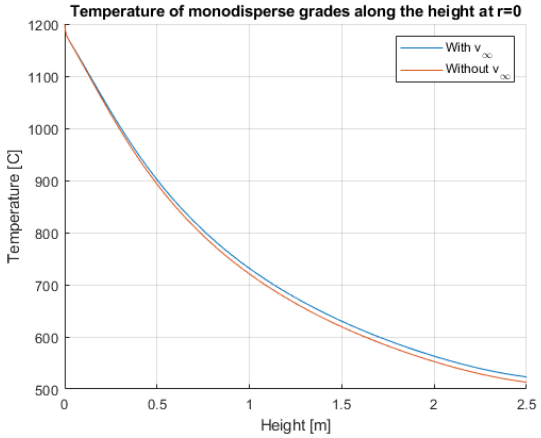

(d) Particle with a diameter of 45 μm.

Figure B.3: Temperature of the mono-disperse grade where the terminal velocity (v_∞) is taken out.

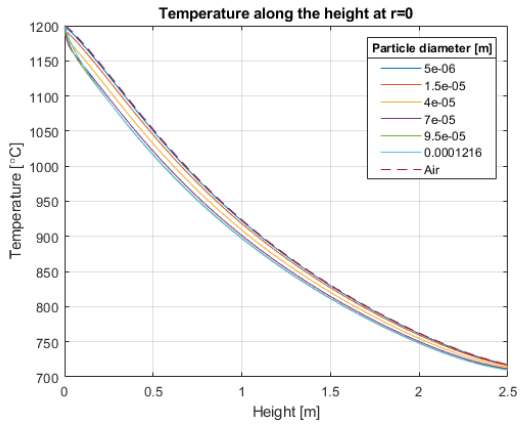

(a) Temperature where the diameter of all particles has been adjusted with -5 μm.

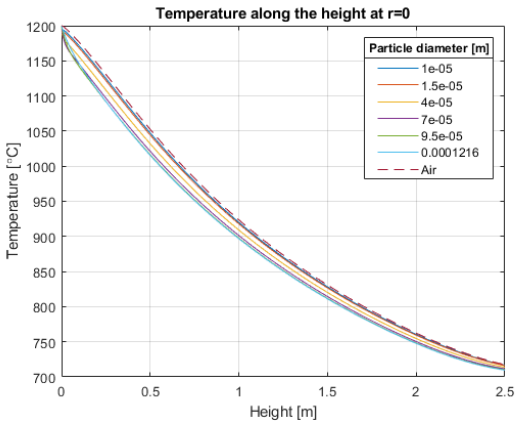

(b) Temperature where the diameter of all particles has been adjusted with -5 μm except the smallest one.

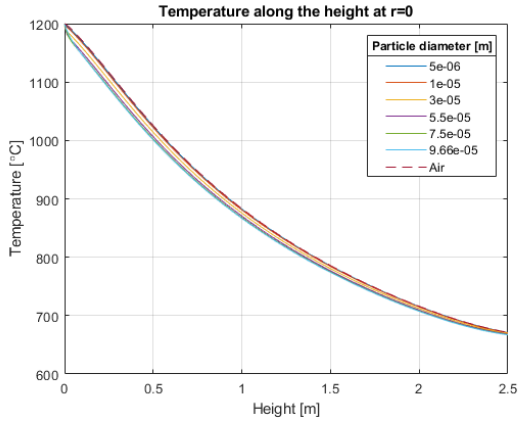

(c) Temperature where the diameter has been adjusted with an increasing value starting with the smallest particle.

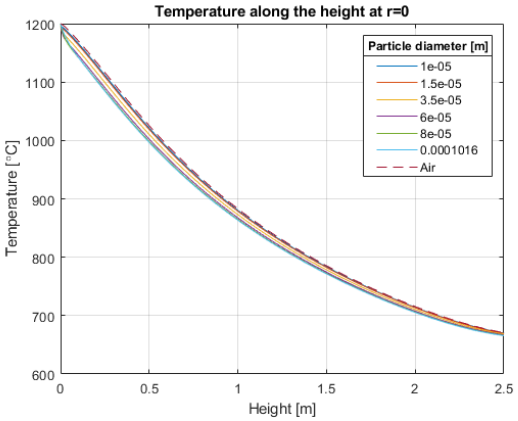

(d) Temperature where the diameter has been adjusted with an increasing value starting at the second smallest particle.

Figure B.4: Tests on the distribution of the particle grades on *model 1*.

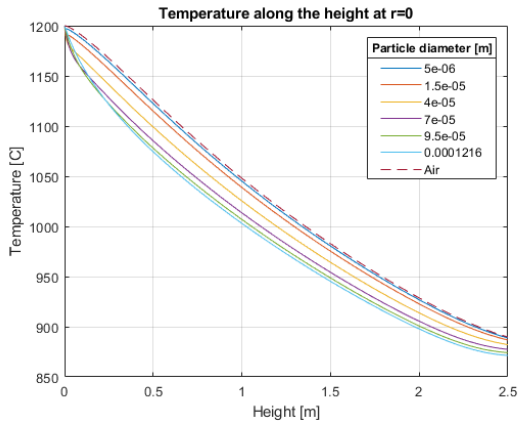

(a) Temperature where the diameter of all particles has been adjusted with -5 μm.

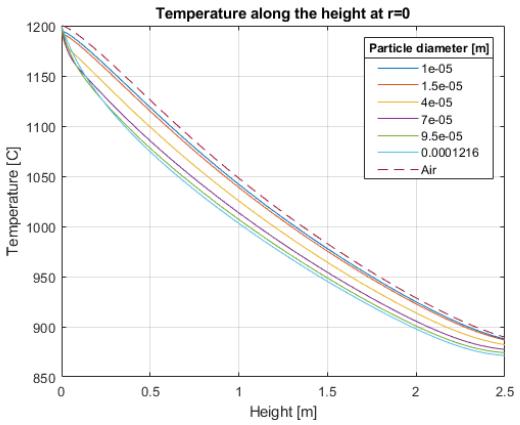

(b) Temperature where the diameter of all particles has been adjusted with -5 μm except the smallest one.

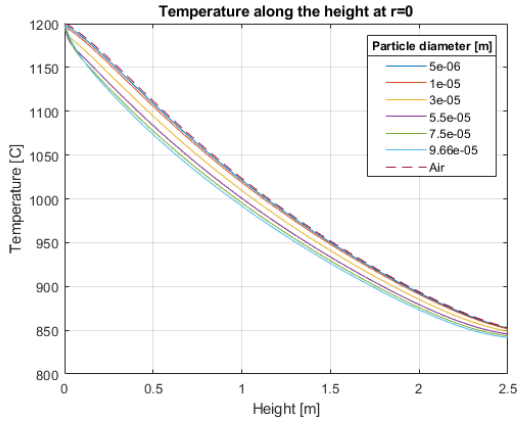

(c) Temperature where the diameter has been adjusted with an increasing value starting with the smallest particle.

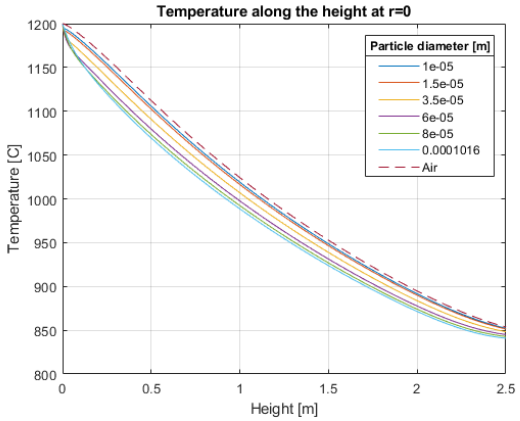

(d) Temperature where the diameter has been adjusted with an increasing value starting at the second largest particle.

Figure B.5: Tests on the distribution of the particle grades on *model 2*.

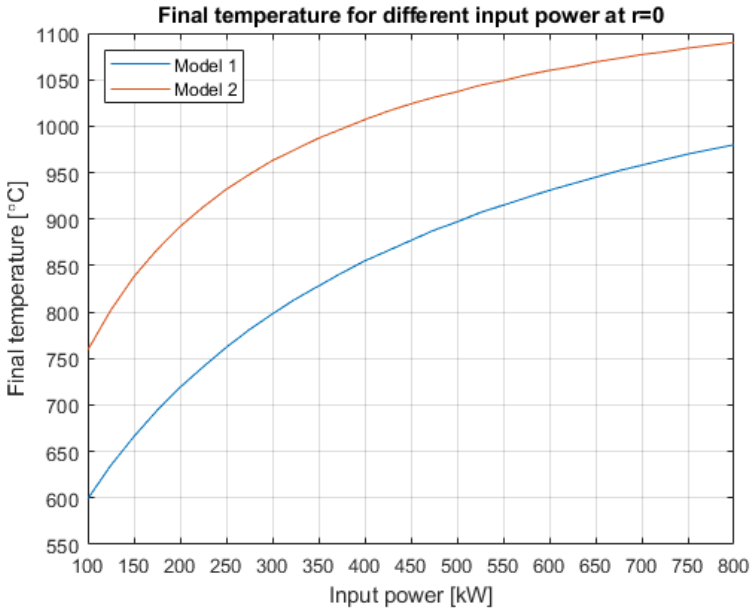

Figure B.6: Final temperature of the air for different input powers.

Table B.3: Values for the variables in *model 2* where the particle tube radius has been changed. (Figure 7.16)

Power input	Heating value	Starting temperature	Steam pipe temperature
200 kW	$5.2 \cdot 10^6$ J/kg	1200 °C	180 °C
Boiler tube radius	Boiler tube length	Specific heat air	Density air
0.5 m	2.5 m	1134 J/kg·K	0.369217 kg/m^2
Viscosity air	Thermal conductivity air	Specific heat Fe2O3	Density iron
$4.0549275 \cdot 10^{-5}$ Pa·s	$6.573 \cdot 10^{-2}$ J/kg·K	654 J/kg·K	7860 kg/m^2
Density Fe2O3	Emissivity iron	Particle tube radius	
5242 kg/m^2	0.85	0.3525 m	

Table B.4: Particle distribution for a larger particle tube. (Figure 7.16)

Diameter [μm]	10	20	40	60	80	100
Number fraction [-]	0.0091	0.1062	0.5134	0.2988	0.0620	0.0105

Table B.5: Values for the variables in *model 2* where the the optimal boiler design is chosen. (Figure 7.18)

Power input	Heating value	Starting temperature	Steam pipe temperature
840 kW	$5.2 \cdot 10^6$ J/kg	1200 °C	180 °C
Boiler tube radius	Boiler tube length	Specific heat air	Density air
1.2 m	2.5 m	1134 J/kg·K	0.369217 kg/m^2
Viscosity air	Thermal conductivity air	Specific heat Fe2O3	Density iron
$4.0549275 \cdot 10^{-5}$ Pa·s	$6.573 \cdot 10^{-2}$ J/kg·K	654 J/kg·K	7860 kg/m^2
Density Fe2O3	Emissivity iron	Particle tube radius	
5242 kg/m^2	0.85	1.0 m	